CMS-HIG-17-012

Search for a new scalar resonance decaying to a pair of Z bosons in proton-proton collisions at $\sqrt{s} = 13\,\text{TeV}$

The CMS Collaboration[*]

Abstract

A search for a new scalar resonance decaying to a pair of Z bosons is performed in the mass range from 130 GeV to 3 TeV, and for various width scenarios. The analysis is based on proton-proton collisions recorded by the CMS experiment at the LHC in 2016, corresponding to an integrated luminosity of $35.9\,\text{fb}^{-1}$ at a center-of-mass energy of 13 TeV. The Z boson pair decays are reconstructed using the 4ℓ, $2\ell2q$, and $2\ell2\nu$ final states, where $\ell = $ e or μ. Both gluon fusion and electroweak production of the scalar resonance are considered, with a free parameter describing their relative cross sections. A dedicated categorization of events, based on the kinematic properties of associated jets, and matrix element techniques are employed for an optimal signal and background separation. A description of the interference between signal and background amplitudes for a resonance of an arbitrary width is included. No significant excess of events with respect to the standard model expectation is observed and limits are set on the product of the cross section for a new scalar boson and the branching fraction for its decay to ZZ for a large range of masses and widths.

*See Appendix A for the list of collaboration members

arXiv:1804.01939v2 [hep-ex] 4 Jul 2018

1 Introduction

The standard model (SM) of particle physics postulates the existence of a single Higgs boson as the manifestation of a scalar field responsible for electroweak (EW) symmetry breaking [1–7]. The ATLAS and CMS Collaborations have discovered a boson with a mass close to 125 GeV [8–10] with properties consistent with those expected for the SM Higgs boson [11–15], and no other fundamental particle that would require explanation beyond the SM (BSM) has been discovered to date. Nonetheless, searches for BSM physics are motivated by a number of phenomena such as the presence of dark matter or baryon asymmetry in the universe that are not explained by the SM. Extensions of the SM that attempt to address these questions include two-Higgs-doublet models (2HDM) [16], of which supersymmetry is an example, or other models predicting an extended Higgs-like EW singlet [17]. In the following, we denote the recently discovered scalar boson as H(125). The search for a heavy scalar partner of the H(125), which we will generically denote as X, is the subject of this paper.

The ZZ decay has a sizable branching fraction for a SM-like Higgs boson for masses larger than the Z boson pair production threshold, $2m_Z$, and is one of the main discovery channels for masses less than $2m_Z$ [8–10]. Since the mass of a new state X is unknown, the search is performed over a wide range of masses from 130 GeV up to 3 TeV. Three final states are considered: 4ℓ, $2\ell 2q$, and $2\ell 2\nu$, with $\ell = $ e or μ. Previous searches for a new boson decaying to ZZ or WW pairs have been reported by the CMS [18] and ATLAS [19, 20] Collaborations at the CERN LHC, using proton-proton collisions recorded at center-of-mass energies of 7 and 8 TeV, where no significant excess was observed. A data set of proton-proton collisions recorded at a center-of-mass energy of 13 TeV by the CMS experiment in 2016 is used in this analysis, corresponding to an integrated luminosity of 35.9 fb^{-1}.

The approach adopted in this analysis treats a new X boson in a model-independent way. For any given mass m_X of the X boson, both its width Γ_X and production mechanism are assumed to be unknown. In this analysis, m_X and Γ_X refer to the mass and width of the scalar boson that enter the propagator. No modification from the complex-pole scheme [21, 22] is considered. The two dominant production mechanisms of a scalar boson are gluon fusion (ggF) and EW production, the latter dominated by vector boson fusion (VBF) with a small contribution of production in association with an EW boson ZH or WH (VH). We define the parameter f_{VBF} as the fraction of the EW production cross section with respect to the total cross section. The three parameters m_X, Γ_X, and f_{VBF} are scanned over a wide range of allowed phase space, and limits are set on the pp $\rightarrow$ X $\rightarrow$ ZZ cross section.

The new state X can potentially have a large value Γ_X: in this case, there is sizable interference between the X $\rightarrow$ ZZ $\rightarrow$ 4f amplitude and that of the SM background process ZZ/Z$\gamma^* \rightarrow$ 4f, where f denotes any fermion. The interference distorts both the kinematic distributions and overall yield of the BSM contribution. The SM background includes the contribution from the H(125) $\rightarrow$ ZZ $\rightarrow$ 4f decays, which yields a nonnegligible off-shell contribution above the $2m_Z$ threshold [21]. The above interference effect is present in both ggF and EW processes and is taken into account in this analysis. The reported cross-section limits correspond to the signal-only contribution as it would be in the absence of interference. A novel feature in this analysis is the inclusion of all of the above effects in a parametric way in a likelihood fit to the data. The matrix element (ME) formalism is used both for the parameterization of the likelihood and for the construction of the observables optimal for event categorization.

The paper is organized as follows. In Section 2, the CMS detector and event reconstruction techniques are presented. Monte Carlo (MC) simulation of the signal and background processes is described in Section 3. Matrix element methods are discussed in Section 4. Event selection and

categorization in each channel are presented in Section 5. Modeling of the signal distributions and background estimation techniques are described in Section 6. Systematic uncertainties are summarized in Section 7. In Section 8 results are presented, and we conclude in Section 9.

2 The CMS detector and event reconstruction

The CMS detector comprises a silicon pixel and strip tracker, a lead tungstate crystal electromagnetic calorimeter (ECAL), and a brass and scintillator hadron calorimeter (HCAL), each composed of a barrel and two endcap sections, all within a superconducting solenoid of 6 m internal diameter and providing a magnetic field of 3.8 T. Outside of the solenoid are the gas-ionization detectors for muon measurements, which are embedded in the steel flux-return yoke outside the solenoid. The detection layers are made using three technologies: drift tubes, cathode strip chambers, and resistive-plate chambers. Extensive forward calorimetry complements the coverage provided by the barrel and endcap detectors. A more detailed description of the CMS detector, together with a definition of the coordinate system and the relevant kinematic variables used, can be found in Ref. [23].

The particle-flow (PF) event algorithm [24] reconstructs and identifies each individual particle with an optimized combination of information from the various elements of the CMS detector. The reconstructed vertex with the largest value of summed physics-object p_T^2 is taken to be the primary pp interaction vertex. The physics objects are the jets, clustered using the jet finding algorithm [25, 26] with the tracks assigned to the vertex as inputs, and the associated missing transverse momentum, taken as the negative vector sum of the p_T of those jets. The energy of photons is obtained from the ECAL measurement, corrected for zero-suppression effects. The energy of electrons is determined from a combination of the electron momentum at the primary interaction vertex as determined by the tracker, the energy of the corresponding ECAL cluster, and the energy sum of all bremsstrahlung photons spatially compatible with originating from the electron track. The momentum of muons is obtained from the curvature of the corresponding tracks in the tracker and the muon systems [27]. The energy of charged hadrons is determined from a combination of their momentum measured in the tracker and the matching ECAL and HCAL energy deposits, corrected for zero-suppression effects and for the response function of the calorimeters to hadronic showers. Finally, the energy of neutral hadrons is obtained from the corresponding corrected ECAL and HCAL energy. The missing transverse momentum vector $\vec{p}_T^{\,\mathrm{miss}}$ is defined as the projection onto the plane perpendicular to the beam axis of the negative vector sum of the momenta of all reconstructed particle-flow objects in an event. Its magnitude is referred to as p_T^{miss}. The correction mentioned above also applies to the determination of p_T^{miss}.

Collision events are selected by high-level trigger algorithms [28] that require the presence of leptons passing loose identification and isolation requirements. The main triggers for this analysis select a pair of electrons or muons. Triggers selecting an eμ pair are also used for the 4ℓ channel and in control samples for 2ℓ2q and 2ℓ2ν. The minimal p_T of the leading electron (muon) is 23 (17) GeV, while that of the subleading lepton is 12 (8) GeV. Isolated single-electron (muon) triggers with minimal p_T of 27 (22) GeV are also employed to complement the double-lepton triggers.

Electrons are measured in the ECAL in the pseudorapidity range $|\eta| < 2.4$. The momentum resolution for electrons with $p_T \approx 45$ GeV from Z $\to$ ee decays ranges from 1.7% for nonshowering electrons in the barrel region to 4.5% for showering electrons in the endcaps [29]. Muons are measured in the range $|\eta| < 2.4$. Muons are reconstructed by combining information from the silicon tracker and the muon system [27]. The matching between the inner and outer tracks

proceeds either outside-in, starting from a track in the muon system, or inside-out, starting from a track in the silicon tracker. In the latter case, tracks that match track segments in one or two (out of four) layers of the muon system are also considered in the analysis to collect very low p_T muons that may not have sufficient energy to penetrate the entire muon system. Matching muons to tracks measured in the silicon tracker results in a relative p_T resolution for muons with $20 < p_T < 100\,\mathrm{GeV}$ of 1.3–2.0% in the barrel and better than 6% in the endcaps. The p_T resolution in the barrel is better than 10% for muons with p_T up to 1 TeV [27].

Hadronic jets are clustered from the four-momenta of the particles in a jet reconstructed by the PF algorithm, using the FASTJET software package [26]. Jets are clustered using the anti-k_T algorithm [25] with a distance parameter equal either to 0.4 ("AK4 jets") or 0.8 ("AK8 jets"). Charged PF constituents not associated with the primary vertex are not used in the jet clustering procedure.

Jet energy momentum is determined as the vectorial sum of all particle four-momenta in the jet. Jets are reconstructed in the range $|\eta| < 4.7$. An offset correction is applied to jet energy momenta to account for the contribution from additional proton proton interactions in the same or neighboring bunch crossings (pileup). These corrections are derived from simulation, and are confirmed with in situ measurements of the energy momentum balance in dijet, multijet, $\gamma + \mathrm{jet}$ and leptonically decaying $Z + \mathrm{jets}$ events [30]. Additional selection criteria are applied to each event to remove spurious jet like features originating from isolated noise patterns in certain HCAL regions.

3 Monte Carlo simulation

Signal events with SM like couplings are generated at next to leading order (NLO) in quantum chromodynamics (QCD) with POWHEG 2.0 [31–35] for the ggF and VBF production modes. The decays $X \rightarrow ZZ \rightarrow 4\ell$, $2\ell 2q$, and $2\ell 2\nu$ are modeled with JHUGEN 7.0.2 [36–39], including corrections for the ZZ branching fraction, and correct modeling of the angular correlation among the fermions. A wide range of masses m_X from $100\,\mathrm{GeV}$ to $3\,\mathrm{TeV}$ is generated with the width Γ_X set according to the SM Higgs boson expectation for m_X up to 1 TeV. For higher masses, we choose the width $\Gamma_X = 0.5 m_X$, which approximately corresponds to the SM Higgs boson prediction for $m_X = 1\,\mathrm{TeV}$. The samples are used to derive a generic signal parameterization.

While NLO accuracy in QCD is used in production, no modeling of the interference with background is included at this stage of the simulation. The MELA matrix element package [36–39], based on JHUGEN for both H(125) and X signal, and on MCFM 7.0 [40–42] for the continuum background, allows modeling of interference of a broad X resonance with SM background in either ggF or EW production, the latter including VBF and VH processes.

The loop induced production of two Z bosons, $\mathrm{gg} \rightarrow ZZ/Z\gamma^* \rightarrow 4f$ background, including the off shell tail of the H(125), is modeled at leading order (LO) in QCD with MCFM. The corresponding background from EW production, $\mathrm{qq'}ZZ/Z\gamma^* \rightarrow 4fqq'$ is modeled at LO in QCD with PHANTOM 1.2.8 [43]. For both ggF and VBF simulation, the factorization and renormalization scales are chosen as $m_{ZZ}/2$, and NNPDF3.0 parton distribution functions (PDFs) [44] are adopted. In order to include higher order QCD corrections to gluon fusion production, LO, NLO, and next to next to leading order (NNLO) signal cross section calculations are performed using the MCFM and HNNLO v2 programs [45–47] for a wide range of masses using the narrow width approximation. The ratio between the NNLO and LO, or between the NLO and LO, is used as a weight depending on the 4f invariant mass (K factor). While this procedure is directly applicable for the signal, it is approximate for the background. However, an NLO calculation

is available [48, 49] for the background in the mass range $2m_Z < m_{4\ell} < 2m_t$. There is a good agreement between the NLO K factors calculated for signal and background and any differences set the scale of systematic uncertainties in this procedure, for which we assign a 10% uncertainty. Event yields for the H(125) boson production are normalized to the cross section at NNLO in QCD and NLO in EW for ggF [50] and others taken from Ref. [51].

The MELA package is also used to reweight the POWHEG/JHUGEN, MCFM, or PHANTOM signal samples to model various values of m_X and Γ_X, as well as the interference with the background component.

The background from the production of two Z bosons from quark antiquark annihilation, $q\overline{q} \to ZZ/Z\gamma^* \to 4f$, is evaluated at NLO with POWHEG [52] and MADGRAPH5_aMC@NLO 2.3.2 [53]. The WZ production is generated at LO with PYTHIA 8.212 [54], normalized to NNLO in QCD accuracy [55]. The Z + jets ($Z \to \ell^+\ell^-$) simulation is made of a composite sample comprising a set of exclusive LO samples with various associated parton multiplicities, including a dedicated sample with associated b quark production. These samples are produced at LO with MADGRAPH5_aMC@NLO and corrected to NLO QCD accuracy with a K factor depending on the p_T of the dilepton pair, derived from MADGRAPH5_aMC@NLO simulation at NLO with FxFx merging scheme [56]. The simulation of top quark antiquark pair production, $t\overline{t}$, is performed with POWHEG at NLO in QCD [57].

All generated samples are interfaced with PYTHIA, configured with the CUETP8M1 tune [58] for simulation of parton showers, hadronization, and underlying event effects. All simulated events are further processed with a GEANT4 based description [59] of the CMS detector and reconstructed with the same algorithms as used for data. Supplementary minimum bias (pileup) interactions are added to the simulated events with a multiplicity determined such as to match that observed in data.

4 Matrix element techniques

The ME method in this study is utilized in three ways. First, it is used to apply weights to generated events from various models to avoid having to fully simulate the samples, as discussed in Section 3. Second, the ME method is used to create a model of a broad high mass resonance X, including its interference with the SM background, to be used in the likelihood fit. Finally, this method is used to create optimal discriminants for either categorization of events according to likely production mechanism, or to separate signal from the dominant background.

The ME calculations are performed using the MELA package, which provides the full set of processes studied in this paper and uses JHUGEN matrix elements for the signal and MCFM matrix elements for the background. The signal includes both the four fermion kinematic properties for the decay $X \to ZZ \to 4f$, and the kinematical properties of associated particles in the X + 2jets, VBF, ZH, WH production. The background includes gg or $q\overline{q} \to ZZ / Z\gamma^* / \gamma^*\gamma^* / Z \to 4f$ processes, VBF production of a Z boson pair, the associated production of a Z pair with a third vector boson, and the production of a single Z boson in association with jets.

Two of the final states studied in this analysis, $X \to ZZ \to 4\ell$ and $2\ell2q$ provide full information about the kinematic properties of the process in both production and decay. This is illustrated in Fig. 1, where a complete set of angles and invariant masses, denoted as $\vec{\Omega}$, fully defines the four vectors of all involved particles in the center of mass frame [36, 38]. The overall boost of the system depends on QCD effects beyond LO (in the transverse plane) or PDFs (in the longitudinal direction). Therefore, in these two channels, matrix element calculations are used

to create discriminants optimal either for categorization of the production mechanism or to separate signal from background using production and decay information.
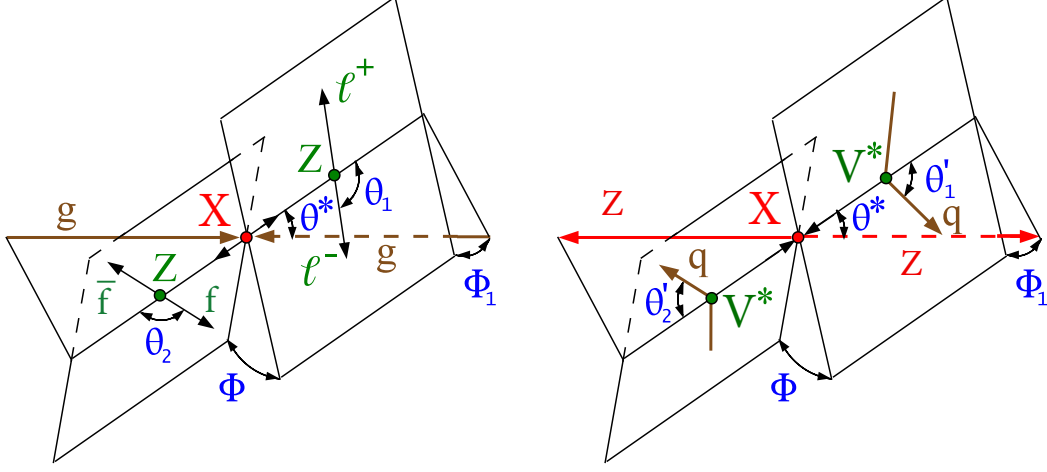

Figure 1: Illustration of an X boson production from ggF, $gg \to X \to ZZ \to (\ell^+\ell^-)(f\bar{f})$ (left), and VBF, $qq' \to qq'X \to qq'ZZ$ (right). The five angles shown in blue and the invariant masses of the two vector bosons shown in green fully characterize either the production or the decay chain. The angles are defined in either the X or V boson rest frames [36, 38].

The discriminant sensitive to the VBF signal topology with two energetic and forward associated jets is calculated as [18, 60]

$$\mathcal{D}_{2\text{jet}}^{\text{VBF}} = \left[1 + \frac{\mathcal{P}_{\text{XJJ}}(\vec{\Omega}^{\text{X+JJ}}|m_{ZZ})}{\mathcal{P}_{\text{VBF}}(\vec{\Omega}^{\text{X+JJ}}|m_{ZZ})} \right]^{-1}, \tag{1}$$

where $\mathcal{P}_{\text{VBF}}$ and $\mathcal{P}_{\text{XJJ}}$ are probabilities obtained from the JHUGEN matrix elements for the VBF and ggF production processes in association with two jets (X + 2 jets). This discriminant is equally efficient in separating VBF from either $gg \to X + 2$ jets signal or gg or $q\bar{q} \to 2\ell2q + 2$ jets background because jet correlations in these processes are distinct from the VBF process. Being independent of the type of fermions produced in the Z boson decay, it is used in both the $X \to ZZ \to 4\ell$ and $X \to ZZ \to 2\ell2q$ analyses.

In addition, in the $X \to ZZ \to 4\ell$ analysis, the dominant background originates from the $q\bar{q} \to ZZ / Z\gamma^* / \gamma^*\gamma^* \to 4\ell$ process. Therefore, the discriminant sensitive to the $X \to ZZ \to 4\ell$ kinematic properties and optimal for suppression of the dominant background is defined as

$$\mathcal{D}_{\text{bkg}}^{\text{kin}} = \left[1 + \frac{\mathcal{P}_{q\bar{q} \to 4\ell}(\vec{\Omega}^{X \to 4\ell}|m_{ZZ})}{\mathcal{P}_{X \to 4\ell}(\vec{\Omega}^{X \to 4\ell}|m_{ZZ})} \right]^{-1}. \tag{2}$$

In the $X \to ZZ \to 2\ell2q$ analysis, the dominant background originates from the Z + 2 jets process. Therefore, the discriminant sensitive to the $X \to ZZ \to 2\ell2q$ kinematic properties is calculated as

$$\mathcal{D}_{\text{bkg}}^{\text{Zjj}} = \left[1 + \frac{\mathcal{P}_{\text{Zjj}}(\vec{\Omega}^{X \to 2\ell2q}|m_{ZZ})}{\mathcal{P}_{X \to 2\ell2q}(\vec{\Omega}^{X \to 2\ell2q}|m_{ZZ})} \right]^{-1}. \tag{3}$$

In Eqs. (2) and (3), $\mathcal{P}_{X \to 4\ell}$ and $\mathcal{P}_{X \to 2\ell2q}$ are the probabilities for the signal, while $\mathcal{P}_{q\bar{q} \to 4\ell}$ and $\mathcal{P}_{\text{Zjj}}$ are the probabilities for the dominant background processes.

5 Event selection and categorization

The searches in the three final states cover different mass ranges. The 4ℓ final state has the smallest backgrounds, so the search is performed over the full range from 130 GeV to 3 TeV. The $2\ell2\nu$ final state suffers from large $Z + $ jets background in the low mass region, and the search range is thus restricted to be between 300 GeV and 3 TeV. For the same reason, the $2\ell2q$ final state search is performed between 550 GeV and 3 TeV. Event selections are optimized for the search ranges in each final state.

Leptons are reconstructed as described in Section 2. Electrons are also required to pass identification criteria based on observables sensitive to the bremsstrahlung along the electron trajectory, the geometrical and momentum energy matching between the electron trajectory and the associated energy cluster in the ECAL, the shape of the electromagnetic shower in the ECAL, and variables that discriminate against electrons originating from photon conversions. Independent selection criteria on such observables are applied in the $2\ell2\nu$ channel, while a multivariate discriminant based on them is adopted in the 4ℓ and $2\ell2q$ channel to retain high efficiency for low p_T leptons. Muons are selected among the reconstructed muon track candidates by applying minimal requirements on the track in both the muon and inner tracker system, and requiring small associated energy deposits in the calorimeters. For muon p_T above 200 GeV, the additional lever arm provided by the outer muon detectors becomes a significant advantage; therefore the charge and momentum are extracted from the combined trajectory fit for the outside in muons, while otherwise tracks found in the silicon tracker are used.

Electrons and muons with high p_T are required in the $2\ell2q$ (>24 GeV) and $2\ell2\nu$ (>25 GeV) final states, while low p_T (>7 GeV for electrons and >5 GeV for muons) leptons are also retained in the 4ℓ final state to ensure high efficiency for masses less than $2m_Z$. To suppress nonprompt leptons, the impact parameter in three dimensions of the lepton track, with respect to the primary vertex, is required to be less than 4 times its uncertainty ($|\text{SIP}_{3D}| < 4$).

In addition, an isolation requirement of $\mathcal{I}^\ell < 0.35$ is imposed to select prompt leptons, where the isolation $\mathcal{I}^\ell$ is defined as

$$\mathcal{I}^\ell \equiv \left(\sum p_T^{\text{charged}} + \max \left[0, \sum p_T^{\text{neutral}} + \sum p_T^\gamma - p_T^{\text{PU}}(\ell) \right] \right) / p_T^\ell. \qquad (4)$$

The three involved sums run over the p_T of charged hadrons originating from the primary vertex, of neutral hadrons and of photons in a cone of angular radius $\Delta R = 0.3$ around the lepton direction.

Since the isolation variable is particularly sensitive to energy deposits from pileup interactions, a $p_T^{\text{PU}}(\ell)$ contribution is subtracted, using two different techniques. For muons, we define $p_T^{\text{PU}}(\mu) \equiv 0.5 \sum_i p_T^{\text{PU},i}$, where i runs over the momenta of the charged hadron PF candidates not originating from the primary vertex, and the factor of 0.5 accounts for the fraction of neutral particles. For electrons, an area based subtraction technique [26, 61, 62], as implemented in FASTJET, is used, in which $p_T^{\text{PU}}(e) \equiv \rho A_{\text{eff}}$, where the effective area A_{eff} is the geometric area of the isolation cone scaled by a factor that accounts for the residual dependence of the average pileup as a function of η, and ρ is the median of the energy density distribution of neutral particles within the area of any jet in the event.

In the 4ℓ and $2\ell2q$ final states, an algorithm is used to recover the final state radiation (FSR) from leptons. Photons reconstructed by the PF algorithm within $|\eta_\gamma| < 2.4$ are considered as FSR candidates if they satisfy $p_T^\gamma > 2$ GeV and $\mathcal{I}^\ell < 1.8$ [63]. Associating every such photon to the closest selected lepton in the event, photons that do not satisfy $\Delta R(\gamma, \ell)/(p_T^\gamma)^2 < 0.012$ and $\Delta R(\gamma, \ell) < 0.5$ are discarded. The lowest $\Delta R(\gamma, \ell)/(p_T^\gamma)^2$ photon candidate for every lepton, if

any, is retained. The photons identified as FSR are excluded from any isolation computations.

The momentum scale and resolution for electrons and muons are calibrated in bins of p_T^ℓ and η^ℓ using the decay products of known dilepton resonances. The electron momentum scale in data is corrected with a Z → ee sample, by adjusting the peak of the reconstructed dielectron mass spectrum to that expected from simulation. A Gaussian smearing is applied to electron energies in simulation such that the Z → ee mass resolution agrees with the one observed in data. Muon momenta are calibrated based on a Kalman filter approach [64], using J/ψ meson and Z boson decays.

A "tag-and-probe" technique [65] based on inclusive samples of Z boson events in data is used to correct the efficiency of the reconstruction and selection for prompt electrons and muons in several bins of p_T^ℓ and η^ℓ. The difference in the efficiencies measured in simulation and data is used to correct the selection efficiency in the simulated samples.

The jets in the three analyses must satisfy $p_T^{jet} > 30$ GeV and $|\eta^{jet}| < 4.7$ and be separated from all selected leptons by $\Delta R(\ell/\gamma, jet) > 0.4$. The analyses use b tagged jets of $|\eta^{jet}| < 2.5$ for event categorization and selection, where a b jet is tagged using the combined secondary vertex algorithm [66, 67] based on the impact parameter significance of the tracks associated with the jet, with respect to the primary vertex. The loose working point is used, corresponding to an efficiency of 80% and a mistag rate of 10% for light quark jets.

The main feature distinguishing the two dominant X boson production mechanisms (ggF and VBF) is the presence of associated jets and the kinematic correlation between such jets and the X boson. In order to gain sensitivity to the production process of the X boson, events are split into categories based on such kinematic correlations. In the case of fully reconstructed final states, X → 4ℓ and 2ℓ2q, a ME technique is used to categorize events based on the correlation between the two forward jets and the X boson candidate, while in the 2ℓ2ν final state a simpler correlation between the two jets is used.

Subsequent event selections differ depending on the considered final state and are described for each final state in the following.

5.1 X → ZZ → 4ℓ

The X → ZZ → 4ℓ analysis uses the same selection as in the measurements of the properties of the H(125) boson in the H → ZZ → 4ℓ decay channel [63]. The Z candidates are formed from pairs of leptons of the same flavor and opposite charge (e^+e^-, $\mu^+\mu^-$) and are required to pass the invariant mass selection $12 < m_{\ell^+\ell^-} < 120$ GeV. The flavors of involved leptons define three mutually exclusive channels: 4e, 4μ, and 2e2μ. Z candidates are combined into ZZ candidates, wherein we denote as Z_1 the Z candidate with an invariant mass closest to the nominal Z boson mass [68], and the other Z candidate Z_2. To be considered for the analysis, ZZ candidates have to pass a set of kinematic requirements. The Z_1 invariant mass is required to be larger than 40 GeV. All leptons are separated in angular space by at least $\Delta R(\ell_i, \ell_j) > 0.02$. At least two leptons are required to have $p_T > 10$ GeV and at least one is required to have $p_T > 20$ GeV. In the 4μ and 4e channels, where an alternative $Z_a Z_b$ candidate can be built out of the same four leptons, candidates with $m_{Z_b} < 12$ GeV are removed if Z_a is closer to the nominal Z boson mass than Z_1 is.

In Ref. [63], six categories are defined based on the number and types of particles associated with the H(125) boson. Here we follow the same approach with some optimization specific for a high mass search. Two categories dedicated to the production mechanisms are used: VBF jets and inclusive; to further improve the efficiency in the electron channels at high p_T, a re-

laxed selection electron (RSE) category is added. The $|\text{SIP}_{3D}| < 4$ requirement in the standard electron selection removes fake electrons from photon conversions, which are not dominant at high masses. The requirement becomes the main cause of efficiency losses at high p_T. The second cause of the efficiency loss, particularly at high masses, is the opposite sign lepton charge requirement, as the charge misidentification rate increases with lepton p_T. Thus, a relaxed selection removing both requirements on at most one pair of electrons is applied for $m_{4\ell} > 300\,\text{GeV}$. The detailed categorization is structured as follows:

- **VBF-tagged** requires exactly four leptons selected with regular criteria. In addition, there must be either two or three jets among which at most one is b tagged, or at least four jets and no b tagged jets, and $\mathcal{D}_{2\text{jet}}^{\text{VBF}}$ following Eq. (1) is required to pass a mass dependent selection;

- **Untagged** consists of the remaining events with regularly selected leptons;

- **RSE** contains events from the relaxed electron selection that are not in the regular electron selection and for which $m_{4\ell} > 300\,\text{GeV}$.

When more than two jets pass the selection criteria, which happens in about half of the cases, the two p_T-leading jets are selected for matrix element calculations.

As a result of the above categorization, events are split into eight categories: 4e, 4μ, 2e2μ, in either the VBF-tagged or the untagged category, or 4e and 2e2μ in the RSE category. Each event is characterized by two observables ($m_{4\ell}$ and $\mathcal{D}_{\text{bkg}}^{\text{kin}}$) that are shown in Fig. 2 and Fig. 3, together with several signal hypotheses.

5.2   X $\rightarrow$ ZZ $\rightarrow$ 2ℓ2q

In the X $\rightarrow$ ZZ $\rightarrow$ 2ℓ2q analysis, events are selected by combining leptonically and hadronically decaying Z candidates. The lepton pair selection is similar to the four-lepton analysis: pairs of opposite sign and same flavor electrons or muons with invariant mass between 60 and 120 GeV are constructed. A $p_T > 40\,\text{GeV}$ requirement is applied on at least one of the leptons in the pair, and a minimum dilepton p_T of 100 GeV is imposed to reject Drell–Yan events with small hadronic recoil.

Hadronically decaying Z boson candidates (Z_{had}) are reconstructed using two distinct techniques, which are referred to as "resolved" and "merged" in the following. In the resolved case, the two quarks from the Z boson decay form two distinguishable AK4 jets, while in the merged case a single AK8 jet with a large p_T is taken as a Z_{had}.

In the merged jet case, a pruning algorithm is applied to the AK8 jet [69, 70]. The goal of the algorithm is to recluster the jet constituents, while applying additional requirements that eliminate soft, large angle QCD radiation that artificially increases the jet mass relative to the nominal Z boson mass. We adopt the unified nomenclature $m(Z_{\text{had}})$ to refer to the hadronically decaying Z candidate mass, corresponding to the dijet invariant mass in the resolved case and the jet pruned mass in the merged case. The reconstructed Z_{had} is required to have an invariant mass around the Z boson mass: $40 < m(Z_{\text{had}}) < 180\,\text{GeV}$ and $p_T > 100\,(170)\,\text{GeV}$ in the resolved (merged) case. Merged jets must also be separated from all selected leptons by $\Delta R(\ell, \text{jet}) > 0.8$. In addition, in the merged jet selection we exploit substructure techniques commonly used in searches including Lorentz boosted bosons in the final state [71]. The N-subjettiness τ_N is defined as

$$\tau_N = \frac{1}{d_0} \sum_k p_{T,k} \min(\Delta R_{1,k}, \Delta R_{2,k}, \ldots, \Delta R_{N,k}), \qquad (5)$$
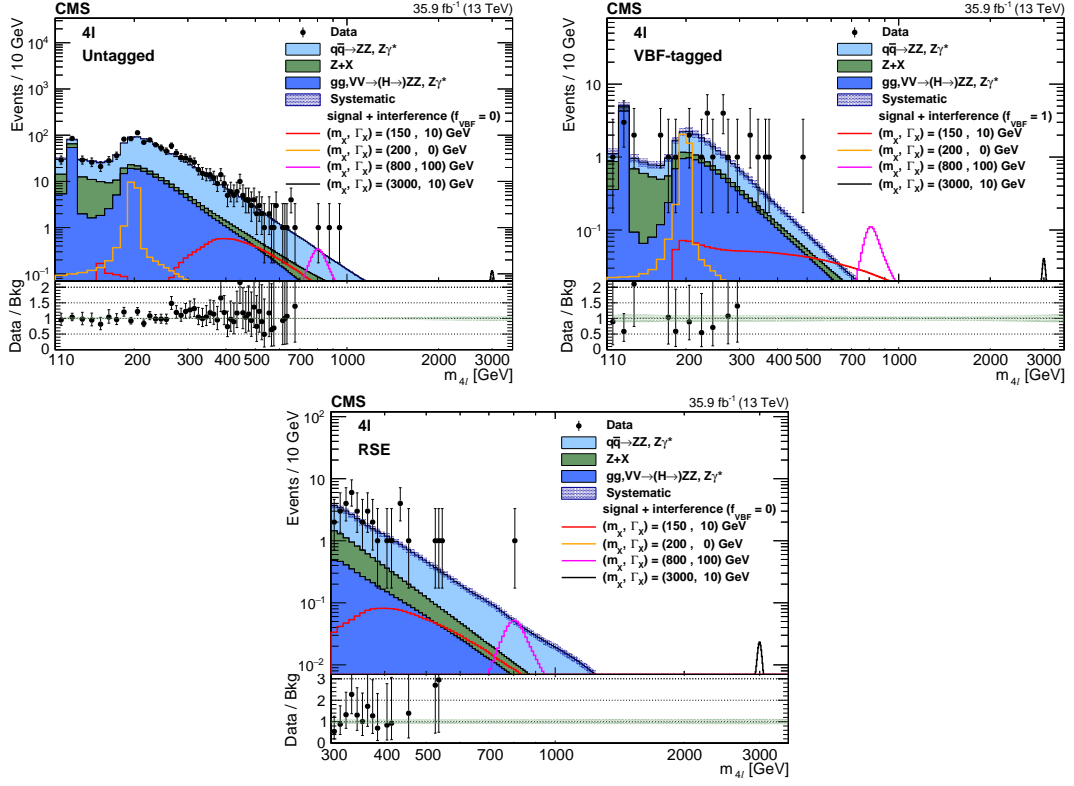
Figure 2: Distributions of the four lepton invariant mass in the untagged (upper left plot), VBF-tagged (upper right plot) and RSE (lower plot) categories. Signal expectations including the interference effect for several mass and width hypotheses are shown. The signals are normalized to the expected upper limit of the cross section derived from this final state. Lower panels show the ratio between data and background estimation in each case.
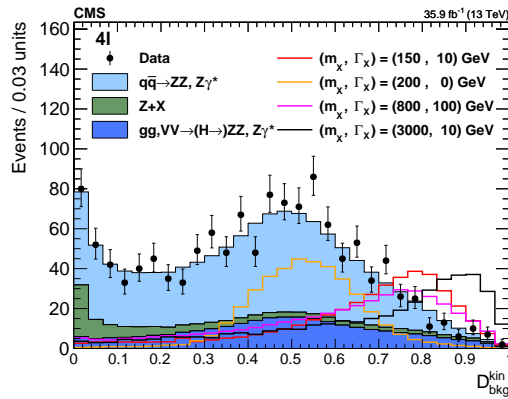

Figure 3: Distributions of $\mathcal{D}_{\text{bkg}}^{\text{kin}}$ for all selected events. Signal expectations including the interference effect for several mass and width hypotheses are shown. The signals are normalized to a total of 400 events.

where the index k runs over the jet constituents and the distances $\Delta R_{N,k}$ are calculated with respect to the axis of the nth subjet. The normalization factor d_0 is calculated as $d_0 = \sum_k p_{\text{T},k} R_0$, setting R_0 to the jet radius of the original jet. Jets with smaller τ_N are more compatible with the N-subjets configuration. We use the ratio of 2-subjettiness over 1-subjettiness, $\tau_{21} = \tau_2/\tau_1$, as the discriminating variable for the jet substructure and impose a $\tau_{21} < 0.6$ requirement on merged Z_{had} candidates.

Events that pass the above selection and additionally have $m(Z_{\text{had}})$ in the range $[70, 105]\,\text{GeV}$ form the signal region, covering 1–2 standard deviations dijet mass resolution. On the other hand, events that have $m(Z_{\text{had}})$ in the range $[40, 70]\,\text{GeV}$ or $[135, 180]\,\text{GeV}$ form the sideband regions and are retained for background estimation.

An arbitration procedure is used to rank multiple Z_{had} candidates reconstructed in a single event: merged candidates have precedence over resolved candidates if they have $p_{\text{T}} > 300\,\text{GeV}$ and the accompanying leptonically decaying Z candidate has $p_{\text{T}}(\ell^+\ell^-) > 200\,\text{GeV}$; resolved candidates have precedence otherwise. Within each selection category the candidate with the largest p_{T} has priority over the others.

The hadronically and leptonically decaying Z boson candidates are combined to form a resonance candidate. In order to improve the ZZ invariant mass resolution in the resolved jet case, a kinematic fit is performed using a mass constraint on the intermediate decay $Z \to q\bar{q}$. The constraint improves the signal resolution by 7–10%. When a candidate belongs to the signal region, we reevaluate the kinematical distributions of final state particles (here the p_{T} of the two jets forming the Z boson of the resonance candidate) with a constraint on the reconstructed Z boson mass to follow the Z boson line shape. For each event, the likelihood is maximized and the p_{T} of the jets is updated. After refit, the mass of the Z boson candidate and m_{ZZ} are recalculated. This procedure is not applied to events in the sidebands, where $m(Z_{\text{had}})$ is very different from the nominal Z boson mass.

The reconstructed ZZ candidate mass m_{ZZ} denotes the dilepton + dijet mass $m_{\ell\ell jj}$ in the resolved case and the dilepton + merged jet invariant mass $m_{\ell\ell J}$ in the merged case. A requirement of $m_{ZZ} > 500\,\text{GeV}$ is imposed to reduce the $Z + \text{jets}$ background.

To increase the sensitivity to the different production modes, events are categorized into VBF and inclusive types. Furthermore, since a large fraction of signal events is enriched with b quark jets due to the presence of $Z \to b\bar{b}$ decays, a dedicated category is defined. The definitions are as follows:

- **VBF-tagged** requires two additional and forward jets besides those constituting the hadronic Z boson candidate; a mass dependent selection criterion on $\mathcal{D}_{2\text{jet}}^{\text{VBF}}$ is applied;

- b **tagged** consists of the remaining events with two b tagged jets (in the resolved case) or two b tagged subjets from the hadronic Z boson candidate;

- **Untagged** consists of the remaining events.

As a result of this categorization, events are split into twelve categories: 2e2q or $2\mu2q$, either VBF-tagged, b-tagged, or untagged, and each with either merged jets or resolved jets. Each event is characterized by the two observables $(m_{ZZ}, \mathcal{D}_{\text{bkg}}^{\text{Zjj}})$. Figure 4 shows the invariant mass distribution for merged and resolved events in each category after the selection. Figure 5 shows the $\mathcal{D}_{\text{bkg}}^{\text{Zjj}}$ and $\mathcal{D}_{2\text{jet}}^{\text{VBF}}$ distributions for resolved events in each category together after the selection.
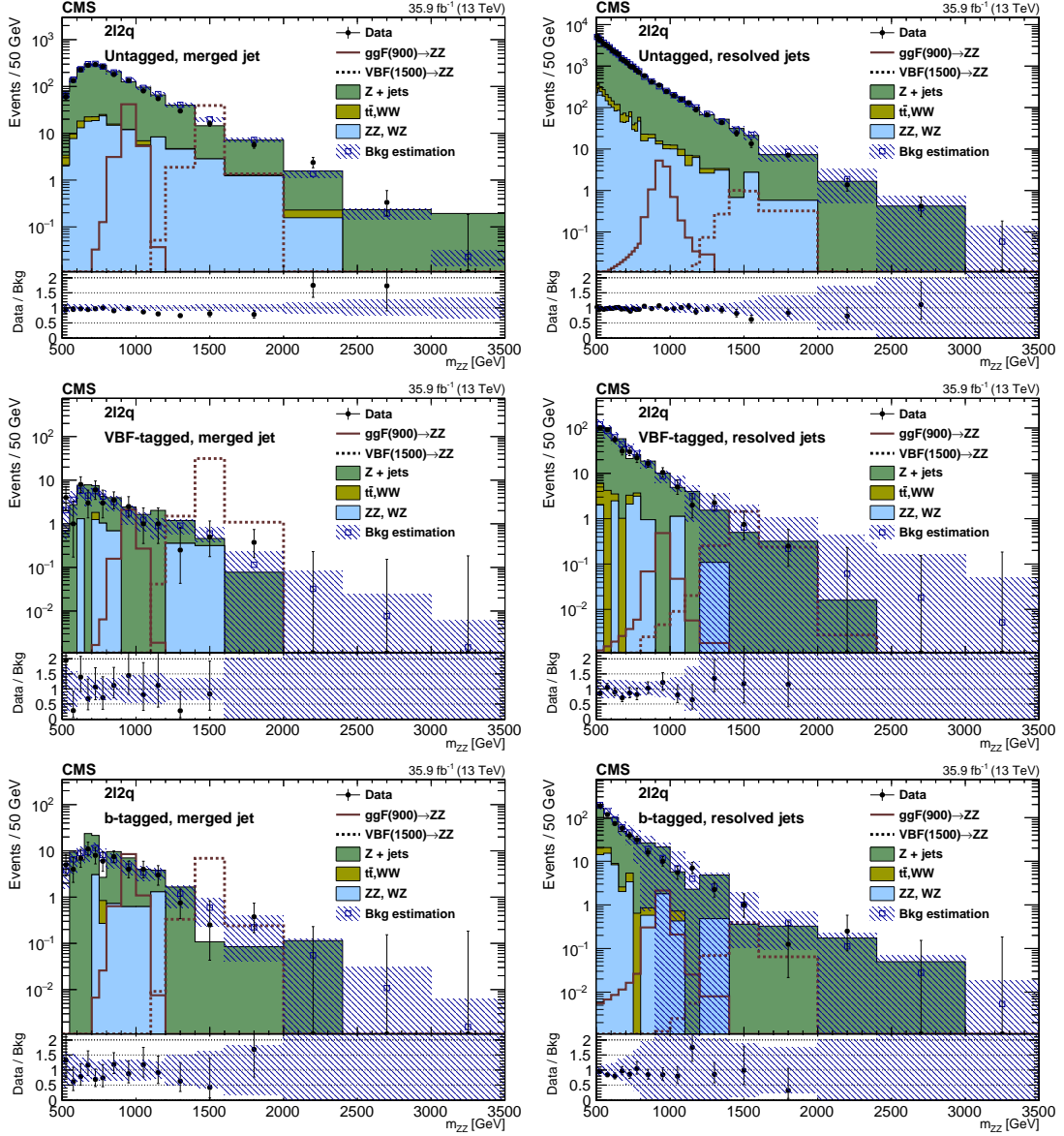
Figure 4: Distributions of the invariant mass m_{ZZ} in the signal region for the merged (left) and resolved (right) case for the different categories in the $2\ell 2q$ channel. The points represent the data, the stacked histograms the expected backgrounds from simulation, and the open histograms the expected signal. The blue hatched bands refer to the sum of background estimates derived from either simulation or control samples in data, as described in the text. Lower panels show the ratio between data and background estimation in each case.
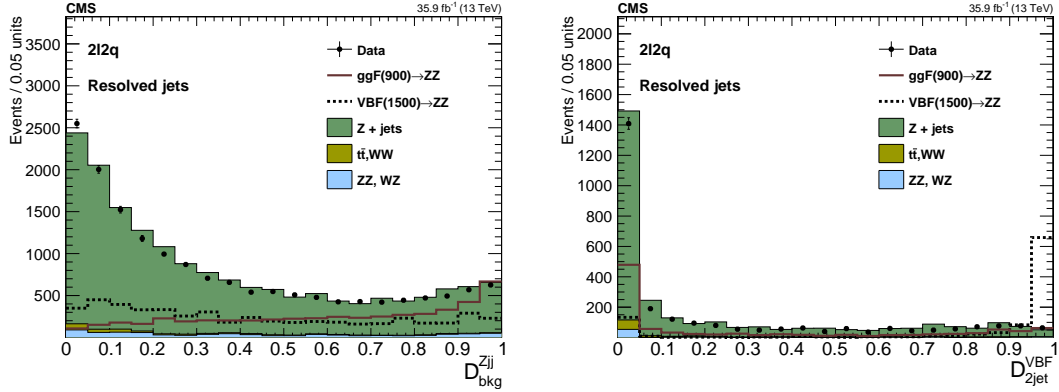
Figure 5: Distributions of the $\mathcal{D}_{bkg}^{Zjj}$(left) and $\mathcal{D}_{2jet}^{VBF}$(right) discriminants in the signal region for the resolved selection. The points represent the data, the stacked histograms the expected background from simulation, and the open histograms the expected signal.

5.3 X → ZZ → 2ℓ2ν

In the $X \to ZZ \to 2\ell 2\nu$ channel, events are selected by combining dilepton Z boson candidates with relatively large p_T^{miss}. Events are selected requiring two leptons of the same flavor that have an invariant mass within a 30 GeV window centered on the nominal Z boson mass. For X boson masses considered in this analysis (>300 GeV), the Z bosons from the X boson decay are typically produced with a large p_T. To suppress the bulk of the Z + jets background, the p_T of the dilepton system is therefore required to be greater than 55 GeV, and a p_T^{miss} threshold of 125 GeV is imposed. The region of large p_T^{miss} is contaminated by Z + jets events in which the p_T^{miss} is largely due to mismeasurements of the jet energies. To suppress this contribution, events are removed if the azimuthal angle between the p_T^{miss} and the closest jet with $p_T >$ 30 GeV is smaller than 0.5 radians. An additional selection requirement $|\Delta\phi(Z, \vec{p}_T^{miss})| > 0.5$ is placed in order to remove events for which the instrumental p_T^{miss} is not well controlled.

Top quark decays are often associated with the production of leptons and missing transverse momentum in the final state but are also characterized by the presence of jets originating from b quarks (b jets). The top quark background is suppressed by applying a veto on events having a b tagged jet with $p_T > 30$ GeV. To reduce the WZ background in which both bosons decay leptonically, any event with an additional e (μ) passing loose identification and isolation criteria with $p_T > 10$ (3) GeV is rejected.

We select events with $p_T^{miss} \geq 125$ GeV and fit the transverse mass m_T distribution for the selected events. The p_T^{miss} requirement rejects background processes that could lead to high m_T because of the kinematic properties of the dilepton pair in the event. The p_T^{miss} criterion is optimized based on expected signal significance. The significance is found to be quite stable with the chosen p_T^{miss} requirement for masses above 400 GeV.

The transverse mass is reconstructed from the dilepton and p_T^{miss} system via the following definition :

$$m_T^2 = \left(\sqrt{p_T(\ell\ell)^2 + m(\ell\ell)^2} + \sqrt{p_T^{miss^2} + m_Z^2} \right)^2 - (\vec{p}_T(\ell\ell) + \vec{p}_T^{miss})^2, \tag{6}$$

where $\vec{p}_T(\ell\ell)$ and $m(\ell\ell)$ are the transverse momentum and invariant mass of the dilepton system, respectively. In order to maximize the sensitivity, the search is carried out in different jet multiplicity categories defined as follows:

- **VBF-tagged**: in this category we require two or more jets in the forward region

with a pseudorapidity gap ($|\Delta\eta|$) between the two leading jets greater than 4, and a minimal invariant mass of those two jets of 500 GeV. The two leptons forming the Z boson candidate are required to lie between these two jets in η, while no other jets ($p_\mathrm{T} > 30$ GeV) are allowed in this central region;

- $\geq$ **1-jet**: events with at least one reconstructed jet with $p_\mathrm{T} > 30$ GeV, but failing the VBF selection;

- **0-jet**: events without any reconstructed jet with $p_\mathrm{T} > 30$ GeV.

The last two categories are the most sensitive to the signal produced via ggF but have different expected signal to background ratios. As a result of the above selection, events are split into six categories: $2e2\nu$ or $2\mu2\nu$, either 0-jet, $\geq$ 1-jet or VBF-tagged. Fig. 6 shows the m_T distributions for the signal and background processes superimposed, in the six event categories.

6 Signal and background parameterization

The goal of the analysis is to determine if a set of X boson parameters m_X, Γ_X, and $\sigma_i\mathcal{B}_{\mathrm{X}\to\mathrm{ZZ}}$ is consistent with the data, where $\sigma_i\mathcal{B}_{\mathrm{X}\to\mathrm{ZZ}}$ is the product of the signal production cross section and the $\mathrm{X}\to\mathrm{ZZ}$ branching fraction in each production channel i (gluon fusion or EW production). In practice, the $\sigma_i\mathcal{B}$ for $i = 1, 2$ are expressed in terms of $\sigma_\mathrm{tot}\mathcal{B}_{\mathrm{X}\to\mathrm{ZZ}}$ and f_VBF, where σ_tot is the sum of the cross sections in the two production channels. The confidence intervals on $\sigma_\mathrm{tot}\mathcal{B}_{\mathrm{X}\to\mathrm{ZZ}}$ are determined from profile likelihood scans for a given set of parameters ($m_\mathrm{X}, \Gamma_\mathrm{X}, f_\mathrm{VBF}$). The extended likelihood function is defined for candidate events as

$$\mathcal{L} = \exp\left(-\sum_i n_{vv}^i - \sum_i n_\mathrm{bkg}^i\right)\prod_k\prod_j\left(\sum_i n_{vv}^i \mathcal{P}_{vv}^{i,k}(\vec{x}_j; m_\mathrm{X}, \Gamma_\mathrm{X}) + \sum_i n_\mathrm{bkg}^i \mathcal{P}_\mathrm{bkg}^{i,k}(\vec{x}_j)\right), \qquad (7)$$

where n_{vv}^i and n_bkg^i are the numbers of signal and background events in channel i. The observables $\vec{x}_j$ are defined for each event j in category k as discussed in Sections 5.1, 5.2, and 5.3. There are several signal and background types i, defined for each production mechanism. The background processes that do not interfere with the signal are described by the probability density functions (pdfs) $\mathcal{P}_\mathrm{bkg}^{i,k}(\vec{x}_j)$. The $vv \to 4f$ process is described by the pdf $\mathcal{P}_{vv}^{i,k}(\vec{x}_j; m_\mathrm{X}, \Gamma_\mathrm{X})$ for $vv = \mathrm{gg}$ (gluon fusion) and $vv = \mathrm{VV}$ (EW production). This pdf describes the production and decay of the X boson signal, SM background, including H(125), and interference between all these contributions and is parameterized as follows:

$$\mathcal{P}_{vv}^{i,k}(\vec{x}_j; m_\mathrm{X}, \Gamma_\mathrm{X}) = \mu_i \mathcal{P}_{vv\to\mathrm{X}\to4f}^{i,k}(\vec{x}_j; m_\mathrm{X}, \Gamma_\mathrm{X}) + \sqrt{\mu_i}\mathcal{P}_\mathrm{int}^{i,k}(\vec{x}_j; m_\mathrm{X}, \Gamma_\mathrm{X}) + \mathcal{P}_{vv\to4f}^{i,k}(\vec{x}_j), \qquad (8)$$

where μ_i is the relative signal strength for production type i defined as the ratio of $\sigma_i\mathcal{B}$ with respect to a reference value, for which normalization of the pdf is determined. The interference contribution $\mathcal{P}_\mathrm{int}^{i,k}$ scales as $\sqrt{\mu_i}$ and the pure signal as μ_i, while both depend on the signal parameters m_X and Γ_X. The likelihood defined in Eq. (7) is maximized with respect to the nuisance parameters, which include the constrained parameters describing the systematic uncertainties.

6.1 Signal model

The parameterization of $\mathcal{P}_{vv}^{i,k}(\vec{x}_j; m_\mathrm{X}, \Gamma_\mathrm{X})$ is performed using the MC simulation discussed in Section 3 with the ME method. In the case of the $\mathrm{X}\to\mathrm{ZZ}\to4\ell$ or $2\ell2\mathrm{q}$ channels, a full reconstruction of the final state is possible. Therefore, the ideal differential distribution prior to detector effects $\mathcal{P}_{vv}^\mathrm{ideal}$, equivalent to Eq. (8), is parameterized using ME techniques and is further corrected for detector acceptance and resolution effects. In the case of $\mathrm{X}\to\mathrm{ZZ}\to$
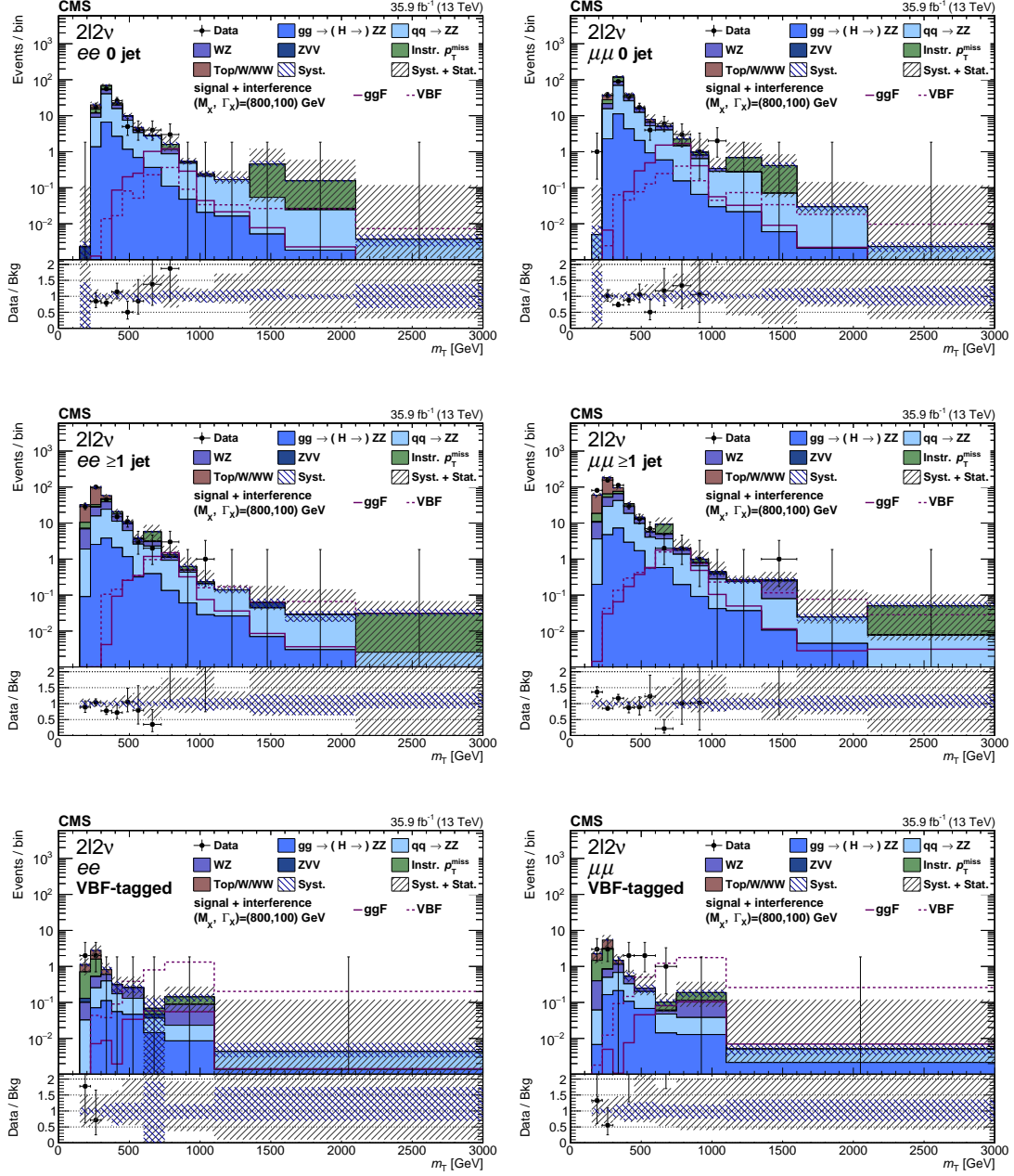
Figure 6: Distributions of the transverse mass m_T in the signal region for the different analysis categories for the $2\ell2\nu$ channel, in the ee(left) and $\mu\mu$ final states (right). The points represent the data and the stacked histograms the expected background. The open histograms show the expected gluon fusion and VBF signals for the product of cross section and branching fraction equal to $\sigma(pp \rightarrow H \rightarrow ZZ) = 50$ fb. Lower panels show the ratio of data to the expected background. The shaded areas show the systematic and total combined statistical and systematic uncertainties in the background estimation.

$2\ell2\nu$, this approach is not possible because of missing neutrinos: MC simulation is reweighted for each hypothesis of m_X, Γ_X, and $\sigma_i\mathcal{B}_{X\to ZZ}$, leading to template parameterization of $\mathcal{P}_{\nu\nu}^{i,k}$ for each set of signal parameters. While ultimately the two approaches are equivalent, the former approach is more flexible in implementation, and the latter avoids the intermediate step of ideal pdf parameterization.

In the $X \to ZZ \to 4\ell$ or $2\ell2q$ channels, we parameterize the signal mass shape as follows. A pdf after detector effects $\mathcal{M}_{\nu\nu}^{\text{reco}}(m_{ZZ})$ is implemented with the multiplicative efficiency function $\mathcal{E}(m_{ZZ})$ and convolved with a mass resolution function $\mathcal{R}(m_{ZZ}|m_{ZZ}^{\text{Gen}})$, both extracted from simulation of the ggF and VBF processes:

$$\mathcal{M}_{\nu\nu}^{\text{reco}}(m_{ZZ}) = \left(\mathcal{E}(m_{ZZ}^{\text{Gen}})\mathcal{M}_{\nu\nu}(m_{ZZ}^{\text{Gen}}|m_X,\Gamma_X) \right) \otimes \mathcal{R}(m_{ZZ}|m_{ZZ}^{\text{Gen}}). \qquad (9)$$

The parameterizations of $\mathcal{R}(m_{ZZ}|m_{ZZ}^{\text{Gen}})$ and $\mathcal{E}(m_{ZZ}^{\text{Gen}})$ cover the mass range from $100\,\text{GeV}$ to $3.5\,\text{TeV}$. Figure 7 shows the efficiencies in the $X \to 4\ell$ and $X \to 2\ell2q$ channels in the various categories. The resolution in the 4ℓ final state is 1–2% and 3–5% in the $2\ell2q$ final state. With the above ingredients, the m_{ZZ} parameterization is shown in Fig. 8, for a boson with $m_X = 450\,\text{GeV}$, $\Gamma_X = 10\,\text{GeV}$ decaying to four leptons. The interference contributions from H(125) and gg $\to$ ZZ background are also shown.
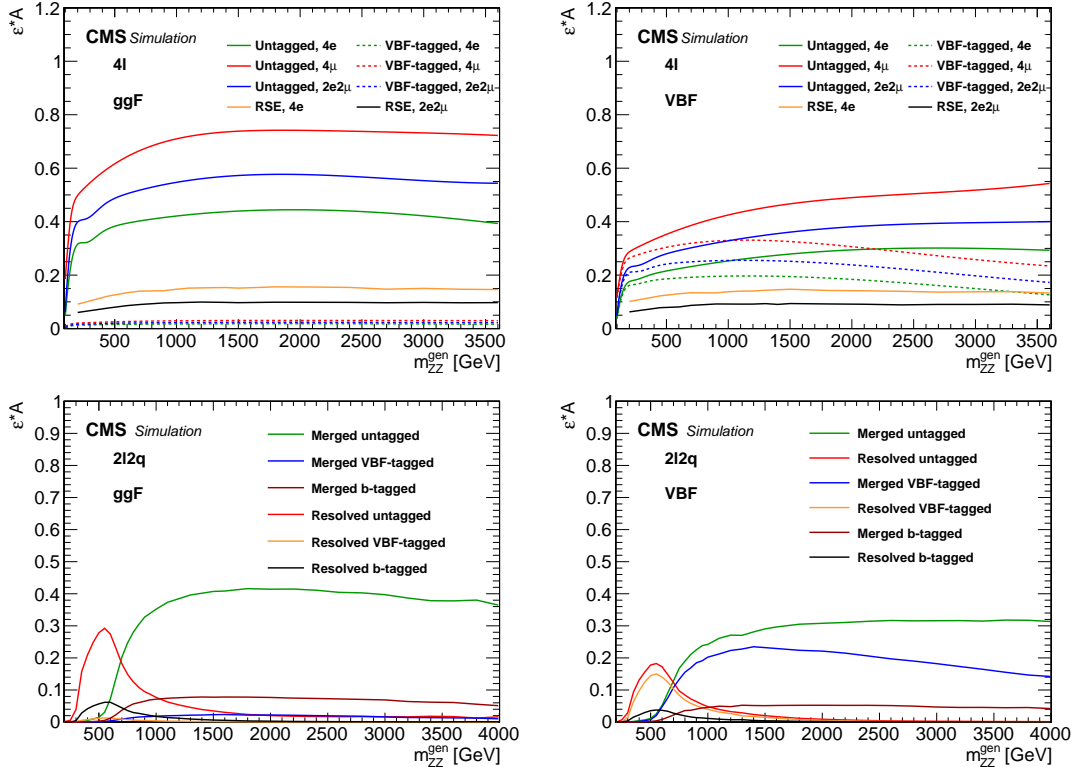
Figure 7: The product of efficiency and acceptance for signal events to pass the $X \to ZZ \to 4\ell$ (upper plots) and $X \to ZZ \to 2\ell2q$ (lower plots) selection as a function of the generated mass m_{ZZ}^{Gen}, from ggF (left) and VBF (right) production modes.

The 2D signal distributions in the 4ℓ and $2\ell2q$ final states are built with the conditional template $\mathcal{T}(D_{\text{bkg}}|m_{ZZ})$, which describes the D_{bkg} discriminant distribution from Eq. (2) or (3) for each value of m_{ZZ}:

$$\mathcal{P}_{vv}^{i,k}(m_{ZZ}, D_{bkg}) = \mathcal{M}_{vv}^{reco}(m_{ZZ})\mathcal{T}(D_{bkg}|m_{ZZ}). \tag{10}$$

The template $\mathcal{T}(D_{bkg}|m_{ZZ})$ parameterization includes all detector effects affecting the D_{bkg} distribution. A closure of the full model described by Eq. (10) is achieved by comparing the model to the simulation for a number of signal parameters.
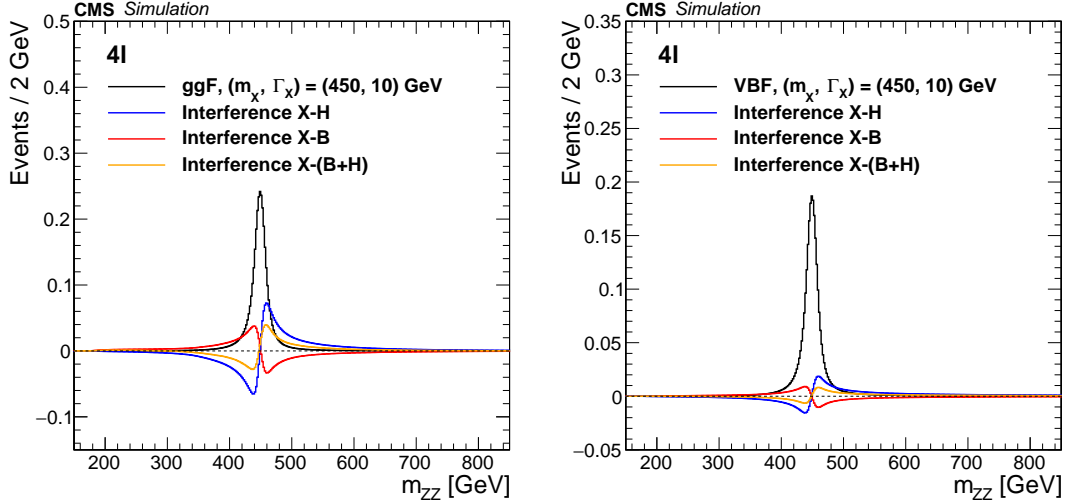

Figure 8: Parameterizations of the four lepton invariant mass for ggF (left) and VBF (right) production modes, for $m_X = 450\,\text{GeV}$, $\Gamma_X = 10\,\text{GeV}$. The interference contributions from H(125) and gg $\rightarrow$ ZZ or VV $\rightarrow$ ZZ background are also shown. The signal cross section used corresponds to the limit obtained in the 4ℓ final state.

6.2 Background model

Common backgrounds among the three final states include the gg(VV) $\rightarrow$ ZZ process, ZZ produced via q$\bar{q}$ annihilation, as well as the WZ production process. The ggF and EW production of the gg(VV) $\rightarrow$ ZZ background are treated together with the X boson signal and background, including interference between the corresponding amplitudes, as discussed in detail in Section 6.1. Higher order corrections are applied to these processes as discussed in Section 3.

The production of ZZ via q$\bar{q}$ annihilation is estimated using simulation. The fully differential cross section for the q$\bar{q}$ $\rightarrow$ ZZ process is computed at NNLO [72], and the NNLO/NLO K factor as a function of m_{ZZ} is applied to the POWHEG sample. This K factor varies from 1.0 to 1.2 and is 1.1 at $m_{ZZ} = 125\,\text{GeV}$. Additional NLO EW corrections, which depend on the flavor of the initial state quarks and on kinematic properties, are also applied in the region $m_{ZZ} > 2m_Z$, where the corrections are computed [73–75]. The WZ production is estimated using simulation, where photon induced EW corrections are applied [76, 77].

The analysis specific background processes, or the ones whose contribution is derived from control samples in data, are discussed in the following sections.

6.2.1 X $\rightarrow$ ZZ $\rightarrow$ 4ℓ

The most important background to the X signal in the 4ℓ channel, in addition to the irreducible ZZ arises from processes in which decays of heavy flavor hadrons, in flight decays of light

mesons within jets, or photon conversion or decay of charged hadrons overlapping with π^0 decays are misidentified as leptons. The main processes producing these backgrounds are $Z +$ jets, $t\bar{t} +$ jets, $Z\gamma +$ jets, $WW +$ jets, and $WZ +$ jets production. Collectively, we denote these as "reducible" backgrounds. The contribution from the reducible background is estimated using two independent methods based on data from dedicated control regions. The control regions are defined by a dilepton pair satisfying all the requirements of a Z_1 candidate and two additional leptons, opposite sign (OS) or same sign (SS), satisfying more relaxed identification criteria than the ones used for the selection and categorization for the signal events. These four leptons are then required to pass the analysis ZZ candidate selection. The event yield in the signal region is obtained by weighting the control region events by the lepton misidentification probability, defined as the fraction of non signal leptons that are identified by the analysis selection criteria.

The lepton misidentification probabilities are measured separately for electrons and muons from a control sample that requires a Z_1 candidate consisting of a pair of leptons, both passing the selection requirements used in the analysis, and exactly one additional lepton passing the relaxed selection.

The predicted yield in the signal region of the reducible background is the result of a combination of the two methods described above. The shape of the $m_{4\ell}$ distribution for the reducible background is obtained by combining the prediction from the OS and SS methods and fitting the distributions with empirical functional forms built from Landau [78] and exponential distributions.

6.2.2 $X \to ZZ \to 2\ell 2q$

The majority of the background ($>90\%$) is composed of events from $Z +$ jets production, where jets associated to the Drell–Yan production are misidentified as coming from a hadronic Z decay. Subdominant backgrounds comprise events from $t\bar{t}$ production and from diboson EW production.

The $t\bar{t}$ background is an important source of contamination in the b tagged category. It is estimated from data using $e^{\pm}\mu^{\mp}$ events passing the same selection as for the signal. This method accounts for other small backgrounds (such as $WW +$ jets, $Z \to \tau^+\tau^- +$ jets, and single top quark production) where the lepton flavor symmetry can be used as well. Because of the limited number of events in the $e^{\pm}\mu^{\mp}$ control region, the m_{ZZ} shapes are taken from $t\bar{t}$ simulation, and the statistical uncertainty in the control region is considered as the uncertainty in the background estimation.

In the $Z+$ jets background, the misidentified hadronic Z comes either from the combinatoric background of $Z + 2$ jets events where the dijet system happens to have an invariant mass in the range compatible with that of the Z boson (resolved category) or from an unusual parton shower and hadronization development for a single jet, leading to a configuration similar to that of the boosted $Z \to q\bar{q}$ decay (merged category). In both cases, and in each analysis category, a sideband region with a misidentified hadronic Z mass close to that of the signal region can be used to estimate the contribution of this background. To address the correlation between the hadronic Z mass and m_{ZZ} in these configurations, a correction factor is estimated from simulation.

The alpha transfer factor $\alpha(m_{ZZ})$, defined as

$$\alpha(m_{ZZ}) = \frac{N_{\mathrm{SIG}}^{\mathrm{MC}}(m_{ZZ})}{N_{\mathrm{SB}}^{\mathrm{MC}}(m_{ZZ})}, \tag{11}$$

is calculated as the ratio of the m_{ZZ} distributions in the signal and sideband regions for $Z + jets$ simulated events. The alpha function is multiplied by the sideband m_{ZZ} distribution to derive the $Z + jets$ contribution in the signal region. The $Z + jets$ distribution from the sideband is obtained by subtracting the subdominant backgrounds from MC prediction. Both the shape and the yield for the $Z + jets$ background are estimated using this method.

While a binned evaluation of the product of the alpha factor and the sideband yields would be a complete estimate of the background, low event yields from data or simulation in specific bins or event categories could induce large statistical fluctuations in the bins with smaller event yields, occurring at large values of m_{ZZ}. We define a "transition" mass value $\tilde{m}_{ZZ}$. For $m_{ZZ} < \tilde{m}_{ZZ}$, the binned evaluation is used as mentioned above. For $m_{ZZ} > \tilde{m}_{ZZ}$, in order to smooth the background estimation, the $Z + jets$ shape is then fit using a sum of two exponential functions (a single exponential function) for the resolved jet untagged category (the remaining categories). A binned estimation for $m_{ZZ} > \tilde{m}_{ZZ}$ is then obtained by integrating the smoothed estimation in the corresponding intervals. The statistical uncertainty derived from the fit is propagated to the final result using the full covariance matrix.

6.2.3 $X \rightarrow ZZ \rightarrow 2\ell 2\nu$

The $Z + jets$ background is modeled from a control sample of events with a single photon produced in association with jets ($\gamma + jets$). This choice has the advantage of making use of a large sample, which captures the source of instrumental p_T^{miss} from the Z production in all important aspects, i.e. production mechanism, underlying event conditions, pileup scenario, and hadronic recoil. By using the $\gamma + jets$ expectation we avoid the need to use the prediction from simulation for the instrumental background arising from the mismeasurement of jets. Each $\gamma + jets$ event must fulfill similar requirements as the dilepton events: no b tagged jets, no additional identified leptons, and a significant transverse momentum ($p_T \geq 55\,GeV$).

The kinematic properties and overall normalization of $\gamma + jets$ events are matched to $Z + jets$ in data through an event by event reweighting as a function of the boson p_T in each of the event categories separately, to account for the dependence of the p_T^{miss} on the associated hadronic activity. Contamination of the photon data by processes that lead to a photon produced in association with genuine p_T^{miss}, such as $W(\ell\nu) + \gamma$ and $W(\ell\nu) + jets$ where the jet is mismeasured as a photon, and $Z(\nu\nu) + \gamma$ events, are subtracted using simulation. The simulation of the p_T^{miss} in such events is more reliable than in $Z + jets$ as the p_T^{miss} is induced by a neutrino and not by detector features. After the p_T reweighting and the p_T^{miss} requirement, these events represent less than 25% of the photon sample. This procedure yields a good description of the p_T^{miss} distribution in $Z + jets$ events, as shown in Fig. 9, which compares the p_T^{miss} distribution of the reweighted $\gamma + jets$ events along with other backgrounds to the p_T^{miss} distribution of the dilepton events in data.

To compute m_T for each $\gamma + jets$ event, $\vec{p}_T^{miss}(\ell\ell)$ is defined as the photon $\vec{p}_T^{miss}$ and the value of $m(\ell\ell)$ is chosen according to a probability density function constructed from the measured dilepton invariant mass distribution in data (dominated by $Z + jets$ events). The uncertainty in this background estimate includes a statistical contribution from the photon control sample and a contribution from the simulations used to subtract processes with photon and genuine p_T^{miss}, and is found to be equal to 100% in the signal region. Another 10% contribution comes from the degree of agreement between the $\gamma + jets$ prediction and the p_T^{miss} distributions in a simulated dilepton sample. Uncertainties in the production cross section of the subtracted processes with genuine p_T^{miss} are also accounted for and are on the order of 25%.

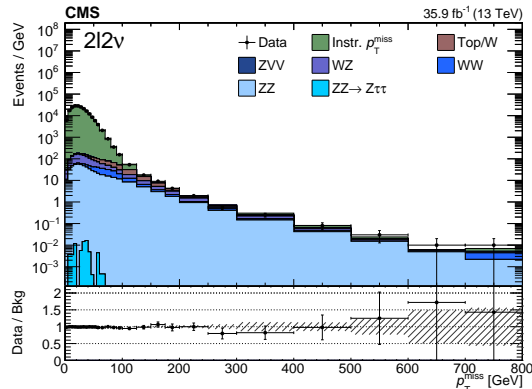The background processes that do not involve a Z resonance (nonresonant background) are

Figure 9: Distribution of the missing transverse energy $p_\mathrm{T}^\mathrm{miss}$ in the dilepton signal region. The points represent the data and the stacked histograms the expected backgrounds. The lower panel shows the ratio between data and background estimation.

estimated using a control sample of events with dileptons of different flavor ($\mathrm{e}^\pm \mu^\mp$) that pass the analysis selection. This background consists mainly of leptonic W decays from $\mathrm{t\bar{t}}$, tW, and WW events. Small contributions from single top quark events produced in s- and t-channels, W + jets events in which the W boson decays leptonically and a jet is mismeasured as a lepton, and ZZ or Z events where a Z decays into τ leptons, which produce light leptons and $p_\mathrm{T}^\mathrm{miss}$, are also included in this estimate. This method cannot distinguish between the nonresonant background and the contribution from $\mathrm{H} \to \mathrm{WW} \to 2\ell 2\nu$ events, which is treated as a part of the nonresonant background estimate. The numbers of nonresonant background events $N_{\mu\mu}$ and N_ee in the $\mathrm{e}^+\mathrm{e}^-$ and $\mu^+\mu^-$ final states are estimated by correcting the number of selected events $N_{\mathrm{e}\mu}$ in the $\mathrm{e}^\pm \mu^\mp$ final state. The correction factor accounts for the difference in branching fractions, acceptance and efficiency between unlike flavor and same flavor dilepton events, and is computed as:

$$N_{\mu\mu} = \frac{N_{\mu\mu}^\mathrm{SB}}{N_{\mathrm{e}\mu}^\mathrm{SB}} N_{\mathrm{e}\mu}, \qquad N_\mathrm{ee} = \frac{N_\mathrm{ee}^\mathrm{SB}}{N_{\mathrm{e}\mu}^{SB}} N_{\mathrm{e}\mu}, \tag{12}$$

where $N_\mathrm{ee}^\mathrm{SB}$, $N_{\mu\mu}^\mathrm{SB}$, and $N_{\mathrm{e}\mu}^\mathrm{SB}$ are the numbers of events in a sideband control sample of $\mathrm{e}^+\mathrm{e}^-$, $\mu^+\mu^-$, and $\mathrm{e}^\pm \mu^\mp$ final states, respectively. The sideband selection is defined by $40 < m(\ell\ell) < 70\,\mathrm{GeV}$ or $110 < m(\ell\ell) < 200\,\mathrm{GeV}$, $p_\mathrm{T}^\mathrm{miss} > 70\,\mathrm{GeV}$, and at least one b tagged jet. The requirement of a b tagged jet is used to provide a sample enriched in top quark events and to suppress possible contamination from Z + jet events where a jet is misidentified as a lepton. The correction factor measured in the sideband is 0.37 ± 0.01 (stat) and 0.68 ± 0.01 (stat) for the ee and $\mu\mu$ channels, respectively. The uncertainty in the estimate of the nonresonant background is determined via MC closure tests using simulated events as well as by comparing results calculated from sideband regions. The total error is within 13%, which is assigned as the systematic uncertainty in this method.

7   Systematic uncertainties

The three final states share common systematic uncertainties arising from the theoretical prediction, reconstructed objects, and common backgrounds. Theoretical uncertainties that affect both the signal and background estimation include uncertainties from the renormalization and factorization scales and the choice of the PDF set. The uncertainties from the renormalization

and factorization scale are determined by varying these scales independently by factors of 0.5 and 2 with respect to their nominal values, while keeping their ratio between 0.5 and 2. The uncertainties from the PDFs are obtained from the root mean squares of the variations, using different replicas of the default NNPDF set. An uncertainty of 10% in the K factor used for the gg → ZZ prediction is applied, which is derived from renormalization and factorization scale variations. The uncertainty in the NNLO-to-NLO K factor for the ZZ and WZ cross sections is about 10%. The renormalization and factorization scale and PDF uncertainties are evaluated from simulation, and are applied to the event categorization and overall signal and background yields. A systematic uncertainty of 2% in the Z boson branching fraction value is taken into account for the signal yields [51].

The uncertainty in the knowledge of the integrated luminosity of the data samples (2.5%) introduces an uncertainty in the numbers of signal and background events passing the final selection. Uncertainties in the lepton identification and reconstruction efficiencies lead to 2.5% uncertainties in the 4μ and 9% in the 4e final states for the 4ℓ selection, 4–8% (2e and 2μ) for $2\ell2$q and 6–8% for $2\ell2\nu$ in the normalizations of both signal and background. The uncertainties in the lepton energy scales are 0.01–0.1% for muons and 0.3% for electrons. A 20% relative uncertainty in the signal resolution is assigned due to per lepton energy resolution in the 4ℓ and $2\ell2$q final states. The jet energy scale (JES), jet energy resolution (JER) and jet reconstruction efficiency uncertainties affect both signal and background yields and represent the most important uncertainties for the $2\ell2$q signal shapes. The systematic uncertainties that are common among the three final states are summarized in Table 1.

Table 1: Sources of uncertainties considered in each of the channels included in this analysis. Uncertainties are given in percent. The numbers shown as ranges represent the uncertainties in different final states or categories. Most uncertainties affect the normalizations of the background estimations or simulated event yields, and those that affect the shape of kinematic distributions as well are labeled with (*).

Source of uncertainty [%]	X → ZZ → 4ℓ	X → ZZ → $2\ell2$q	X → ZZ → $2\ell2\nu$
Experimental sources			
Integrated luminosity	2.5	2.5	2.5
ℓ trigger and selection efficiency	2.5–9	4–8	6–8
ℓ momentum/energy scale (*)	0.04–0.3	0.1–0.3	0.01–0.3
ℓ resolution (*)	20	20	—
JES, JER, $p_\mathrm{T}^\mathrm{miss}$ (*)	1–30	1–10	1–30
b tagging/mistag	—	5–7	2–4
Background estimates			
Z + jets	36–43	10–50	20–50
top quark, WW	—	15	10
Wγ^*, WZ	—	3–10	15
Theoretical sources			
Renorm./factor. scales	3–10	3–10	5–10
PDF set	3–4	3–5	1–4
EW corrections (q$\bar{\mathrm{q}}$ → ZZ) (*)	1	1	2
NNLO (gg → ZZ) K factor	10	10	10

In addition, each final state has channel specific uncertainties, mainly from the background estimations based on control samples in data, as well as from merged jet reconstruction.

7.1   X → ZZ → 4ℓ

Experimental uncertainties for this channel arise mainly from the reducible background esti-
mation. Impacts from the limited numbers of events in the control regions as well as in the
region region where the misidentification rates evaluated are taken into account. Additional
sources of systematic uncertainty arise from the difference in the composition of the sample
from which the misidentification rate is computed and the control regions of the two methods
where the lepton misidentification probability is applied. The systematic uncertainty in the
$m_{4\ell}$ shape is determined by taking the envelope of differences among the shapes from the OS
and SS methods in the three different final states. The combined systematic uncertainties are
estimated to be about 36% (4μ) to 43% (4e).

7.2   X → ZZ → 2ℓ2q

The dominant uncertainties in the signal selection efficiency for this channel arise from uncer-
tainties in the efficiencies to tag the hadronic jet as a Z in the high mass boosted categories,
and from uncertainties in the b tagging efficiency. The efficiency of the boosted boson tagging
selection and its corresponding systematic uncertainty are measured from data using a sam-
ple enriched in t$\bar{\text{t}}$ events. Uncertainties in the signal efficiencies from the jet mass scale and
resolution are 1–9% and 7–13% depending on the mass. τ_{21} selection scale factor and extrap-
olation lead to 8% and 2–8% uncertainties. The b tagging efficiencies and their corresponding
systematic uncertainties are measured from data enriched in t$\bar{\text{t}}$ events. They account for 5–7%
uncertainties in the total signal efficiencies.

For the background estimated from data, the statistical uncertainty of the e$^{\pm}$ $\mu^{\mp}$ control sam-
ple is propagated to an uncertainty in the t$\bar{\text{t}}$+WW estimation. The alpha method for the Z +
jets background estimation depends on the uncertainty in the extrapolation factor and on the
amount of data of the dijet mass or pruned jet mass sideband region. Jet energy scale and reso-
lution affect the extrapolation factor $\alpha(m_{ZZ})$ by 3–10% depending on the mass. In the low mass
region, the statistical uncertainties in the simulated samples and mass sidebands in data are
propagated to the binned alpha factor estimation. In the high mass region, they are obtained
by the covariance matrix of the fit parameters of the sideband data m_{ZZ} distributions. Ad-
ditional systematic uncertainties are derived from comparisons between the nominal Z + jets
MC descriptions (exclusive LO samples with different associated parton multiplicities, and en-
riched in b quark production, all produced with MADGRAPH5_aMC@NLO) and the merged
MADGRAPH5_aMC@NLO simulations at NLO. The same background estimation methods are
used to derive an alternative binned description of the Z + jets background, and appropriate
nuisance parameters, symmetrized around zero, describe the variation between the nominal
and alternative estimation.

For the two dimensional $\mathcal{D}^{Zjj}_{\text{bkg}}$ template shapes, two systematic uncertainties are considered for
the signal samples: JES and JER variations, as well as comparison with identical MC samples
where HERWIG++ [79] with EE5C tune [58] is used for parton showering and hadronization
instead of PYTHIA. For background templates, a conservative systematic uncertainty from the
limited size of the MC samples and the consequent smoothing procedure is derived by using
alternative templates where the content of each two dimensional interval is replaced by the
content of the preceding or following interval in m_{ZZ}. Background systematic uncertainties
are validated in an "extended sideband region", which includes the sideband region used in
the analysis, as well as events failing the τ_{21} selection. At masses above 1 TeV, 1σ differences
between data and simulation in this region are assigned as additional systematic uncertainties.

7.3 $X \to ZZ \to 2\ell2\nu$

Various factors contribute to the experimental uncertainties that apply to processes derived from MC simulation. These include uncertainties in the trigger efficiency and lepton selection efficiencies. The effects of lepton momentum scale and JES are also taken into account and are propagated to the evaluation of p_T^{miss}. The uncertainties in the b jet veto are estimated by measuring the b tagging efficiency in data enriched in $t\bar{t}$ and are evaluated to be 2–4% for processes estimated from simulation, namely signal and WW, WZ events. Uncertainties due to the modeling of pileup are evaluated by varying the total inelastic cross section by $\pm5\%$ around the nominal value.

Uncertainties in the background estimates based on control regions in data are estimated as described in Section 6.2.3. For the Drell–Yan background a systematic uncertainty of 25% is combined with a statistical uncertainty from the size of the photon + jet control sample of 10% for the 0-jet and $\geq$1-jet categories, and of 50% for the VBF-tagged category. For the nonresonant background a 15% uncertainty is applied.

8 Results

The search for a scalar resonance X decaying to ZZ is performed over the mass range $130\,\text{GeV} < m_X < 3\,\text{TeV}$, where three final states are combined, $X \to ZZ \to 4\ell$, $2\ell2q$, and $2\ell2\nu$. Because of the different resolutions, efficiencies, and branching fractions, each final state contributes differently depending on the tested mass. The most sensitive final state between 130 and 500 GeV is 4ℓ due to its best mass resolution, whereas in the intermediate region 500–700 GeV $2\ell2\nu$ is most sensitive, and for masses above 700 GeV $2\ell2q$ is best.

In $X \to ZZ \to 4\ell$ and $2\ell2q$, comparisons between the two dimensional (m_{ZZ}, $\mathcal{D}_{bkg}^{Zjj}$) distributions observed in data and expected from the sum of background predictions are made. We set upper limits on the production cross section of the resonance by combining all the event categories in each analysis.

In $X \to ZZ \to 2\ell2\nu$, using the resulting m_T distributions, a shape based analysis is performed to extract the limits. The shapes of the signal and WZ, ZZ backgrounds are taken from MC simulation, those of Z + jets are taken from data, and for nonresonant backgrounds, the $e\mu$ control region is used to predict both shapes and normalizations of the m_T distributions in the signal region, as described in Section 6.2.

We follow the modified frequentist prescription described in Refs. [80–82] (CL$_s$ method), and an asymptotic approach with the profile likelihood ratio as the test statistic is used for upper limits. Systematic uncertainties are treated as nuisance parameters and profiled using lognormal priors.

The width of the resonance Γ_X is allowed to vary, starting from the narrow width approximation (denoted as $\Gamma_X = 0$) up to a large width. Production of the X resonance is considered to be either in ggF or VBF, where VX production is included according to the relative expectation of the VX and VBF cross sections. No significant excess of events over the SM expectation is observed. Figure 10 shows upper limits at the 95% confidence level (CL) on the pp $\to X \to ZZ$ cross section $\sigma_X \mathcal{B}_{X \to ZZ}$ as a function of m_X for $\Gamma_X = 0, 10$, and 100 GeV.

The expected and observed limits on the pure VBF production cross section are better than the inclusive ones, because the background is smaller in the dedicated VBF categories. In general, limits are better when assuming a narrow width signal, since the signal over background ratio

is higher. However, in the mass region below 300 GeV, interference effects with background are more complicated and play a role in the evolution of the limit as a function of Γ_X.

For $m_X < 2m_Z$, while the signal events are produced on shell around m_X for $\Gamma_X \sim 0$, the majority of the events are produced off shell in the case of $\Gamma_X/m_X > 1\%$. Thus the relevant background is quite different when Γ_X varies. In the ggF dominant category, for $130 < m_X < 140$ GeV, the signal over background ratio is better in the relevant off shell region than in the on shell region, where signal events partly overlap with the H(125) peak. This makes the sensitivity better for a wide resonance. For $150 < m_X < 180$ GeV, there is no overlap between the two on shell resonance peaks, so for a narrow resonance the signal over background ratio is larger and the limit is better. In the VBF category, the signal over background ratio is always smaller in the relevant off shell region compared to the on shell region, yielding a better sensitivity for a wide resonance. The downward fluctuation in the VBF limit for $\Gamma_X = 10$ and 100 GeV, and $m_X < 180$ GeV, reflects an overall deficit of events in the VBF category in the off shell region of $m_{4\ell} > 200$ GeV.

Above the $2m_Z$ threshold, for $180 < m_X < 250$ GeV, the net interference of the ggF signal is positive around the peak, making the wide resonance sensitivity better. For the VBF signal, the enhancement from interference occurs at its right hand tail, where barely any background exists. This makes the limit for the wide VBF Higgs better in the range $m_X < 300$ GeV. Above that, the background drops rapidly and the limits for narrow and wide resonances are compatible.

Figure 11 shows the scan of the observed upper limits at the 95% CL, as a function of m_X and Γ_X/m_X. The mass is scanned from 130 GeV to 3 TeV and the relative width from 0 to 30%. The results are provided with f_{VBF} profiled and fixed to unity. The excluded product of the cross section and branching fraction ranges from 1.2 fb at 3 TeV to 402.6 fb at 182 GeV in the case of f_{VBF} profiled, and from 1.0 fb at 3 TeV to 221.1 fb at 134 GeV in the VBF production mode.

9   Summary

A search for a new scalar resonance decaying to a pair of Z bosons is performed for a range of masses between 130 GeV and 3 TeV with the full data set recorded by the CMS experiment at 13 TeV during 2016 and corresponding to an integrated luminosity of 35.9 fb^{-1}. Three final states ZZ $\to 4\ell$, $2\ell 2q$, and $2\ell 2\nu$ are combined in the analysis, where $\ell = $ e or μ. Both gluon fusion and electroweak production of the scalar resonance are considered with a free parameter describing their relative cross sections. A dedicated categorization of events based on the kinematic properties of the associated jets is used to improve the sensitivity of the search. A description of the interference between signal and background amplitudes for a resonance of an arbitrary width is included. No significant excess of events over the SM expectation is observed and limits are set on the product of the cross section and the branching fraction for its decay to ZZ for a wide range of masses and widths, and for different production mechanisms.
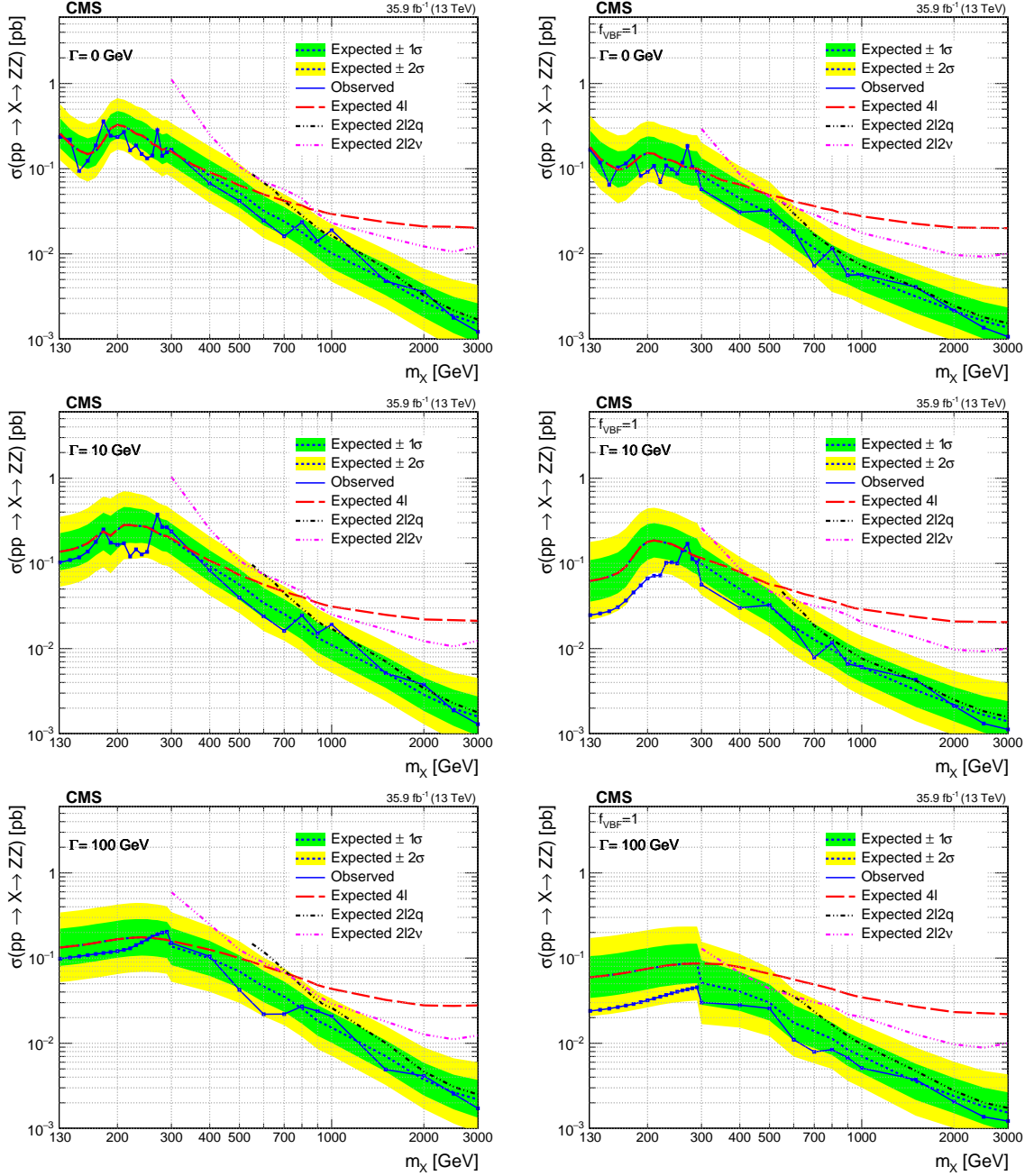
Figure 10: Expected and observed upper limits at the 95% CL on the $pp \rightarrow X \rightarrow ZZ$ cross section as a function of m_X and for several Γ_X values with f_{VBF} as a free parameter (left) and fixed to 1 (right). The results are shown for 4ℓ, $2\ell 2q$, and $2\ell 2\nu$ channels separately and combined. The reported cross section corresponds to the signal only contribution in the absence of interference.
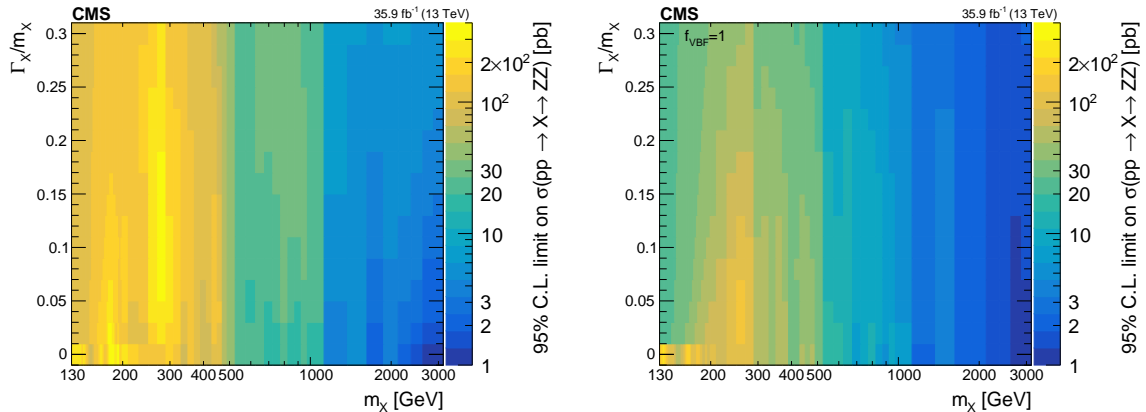
Figure 11: Observed upper limits at the 95% CL on the pp → X → ZZ cross section as a function of m_X and Γ_X/m_X values with f_{VBF} as a free parameter (left) and fixed to 1 (right). The results are shown for the 4ℓ, $2\ell 2q$, and $2\ell 2\nu$ channels combined. The reported cross section corresponds to the signal only contribution in the absence of interference.

References

[1] S. L. Glashow, "Partial-symmetries of weak interactions", *Nucl. Phys.* **22** (1961) 579, `doi:10.1016/0029-5582(61)90469-2`.

[2] F. Englert and R. Brout, "Broken symmetry and the mass of gauge vector mesons", *Phys. Rev. Lett.* **13** (1964) 321, `doi:10.1103/PhysRevLett.13.321`.

[3] P. W. Higgs, "Broken symmetries, massless particles and gauge fields", *Phys. Lett.* **12** (1964) 132, `doi:10.1016/0031-9163(64)91136-9`.

[4] P. W. Higgs, "Broken symmetries and the masses of gauge bosons", *Phys. Rev. Lett.* **13** (1964) 508, `doi:10.1103/PhysRevLett.13.508`.

[5] G. S. Guralnik, C. R. Hagen, and T. W. B. Kibble, "Global conservation laws and massless particles", *Phys. Rev. Lett.* **13** (1964) 585, `doi:10.1103/PhysRevLett.13.585`.

[6] S. Weinberg, "A model of leptons", *Phys. Rev. Lett.* **19** (1967) 1264, `doi:10.1103/PhysRevLett.19.1264`.

[7] A. Salam, "Weak and electromagnetic interactions", in *Elementary particle physics: relativistic groups and analyticity*, N. Svartholm, ed., p. 367. Almqvist & Wiksell, Stockholm, 1968. Proceedings of the eighth Nobel symposium.

[8] ATLAS Collaboration, "Observation of a new particle in the search for the standard model Higgs boson with the ATLAS detector at the LHC", *Phys. Lett. B* **716** (2012) 1, `doi:10.1016/j.physletb.2012.08.020`, `arXiv:1207.7214`.

[9] CMS Collaboration, "Observation of a new boson at a mass of 125 GeV with the CMS experiment at the LHC", *Phys. Lett. B* **716** (2012) 30, `doi:10.1016/j.physletb.2012.08.021`, `arXiv:1207.7235`.

[10] CMS Collaboration, "Observation of a new boson with mass near 125 GeV in pp collisions at $\sqrt{s}$ = 7 and 8 TeV", *JHEP* **06** (2013) 081, `doi:10.1007/JHEP06(2013)081`, `arXiv:1303.4571`.

[11] CMS Collaboration, "Study of the mass and spin-parity of the Higgs boson candidate via its decays to Z boson pairs", *Phys. Rev. Lett.* **110** (2013) 081803, `doi:10.1103/PhysRevLett.110.081803`, `arXiv:1212.6639`.

[12] CMS Collaboration, "Measurement of the properties of a Higgs boson in the four-lepton final state", *Phys. Rev. D* **89** (2014) 092007, `doi:10.1103/PhysRevD.89.092007`, `arXiv:1312.5353`.

[13] CMS Collaboration, "Constraints on the spin-parity and anomalous HVV couplings of the Higgs boson in proton collisions at 7 and 8 TeV", *Phys. Rev. D* **92** (2015) 012004, `doi:10.1103/PhysRevD.92.012004`, `arXiv:1411.3441`.

[14] ATLAS Collaboration, "Evidence for the spin-0 nature of the Higgs boson using ATLAS data", *Phys. Lett. B* **726** (2013) 120, `doi:10.1016/j.physletb.2013.08.026`, `arXiv:1307.1432`.

[15] ATLAS Collaboration, "Study of the spin and parity of the Higgs boson in diboson decays with the ATLAS detector", *Eur. Phys. J. C* **75** (2015) 476, `doi:10.1140/epjc/s10052-015-3685-1`, `arXiv:1506.05669`.

[16] G. C. Branco et al., "Theory and phenomenology of two-Higgs-doublet models", *Phys. Rept.* **516** (2012) 1, `doi:10.1016/j.physrep.2012.02.002`, `arXiv:1106.0034`.

[17] C. Caillol, B. Clerbaux, J.-M. Frére, and S. Mollet, "Precision versus discovery: A simple benchmark", *Eur. Phys. J. Plus* **129** (2014) 93, `doi:10.1140/epjp/i2014-14093-3`, `arXiv:1304.0386`.

[18] CMS Collaboration, "Search for a Higgs boson in the mass range from 145 to 1000 GeV decaying to a pair of W or Z bosons", *JHEP* **10** (2015) 144, `doi:10.1007/JHEP10(2015)144`, `arXiv:1504.00936`.

[19] ATLAS Collaboration, "Search for an additional, heavy Higgs boson in the H → ZZ decay channel at $\sqrt{s} = 8$ TeV in pp collision data with the ATLAS detector", *Eur. Phys. J. C* **76** (2016) 45, `doi:10.1140/epjc/s10052-015-3820-z`, `arXiv:1507.05930`.

[20] ATLAS Collaboration, "Search for a high-mass Higgs boson decaying to a W boson pair in pp collisions at $\sqrt{s} = 8$ TeV with the ATLAS detector", *JHEP* **01** (2016) 032, `doi:10.1007/JHEP01(2016)032`, `arXiv:1509.00389`.

[21] N. Kauer and G. Passarino, "Inadequacy of zero-width approximation for a light Higgs boson signal", *JHEP* **08** (2012) 116, `doi:10.1007/JHEP08(2012)116`, `arXiv:1206.4803`.

[22] S. Goria, G. Passarino, and D. Rosco, "The Higgs boson lineshape", *Nucl. Phys. B* **864** (2012) 530, `doi:10.1016/j.nuclphysb.2012.07.006`, `arXiv:1112.5517`.

[23] CMS Collaboration, "The CMS experiment at the CERN LHC", *JINST* **3** (2008) S08004, `doi:10.1088/1748-0221/3/08/S08004`.

[24] CMS Collaboration, "Particle-flow reconstruction and global event description with the CMS detector", *JINST* **12** (2017) P10003, `doi:10.1088/1748-0221/12/10/P10003`, `arXiv:1706.04965`.

[25] M. Cacciari, G. P. Salam, and G. Soyez, "The anti-k_T jet clustering algorithm", *JHEP* **04** (2008) 063, `doi:10.1088/1126-6708/2008/04/063`, `arXiv:0802.1189`.

[26] M. Cacciari, G. P. Salam, and G. Soyez, "FastJet user manual", *Eur. Phys. J. C* **72** (2012) 1896, `doi:10.1140/epjc/s10052-012-1896-2`, `arXiv:1111.6097`.

[27] CMS Collaboration, "Performance of CMS muon reconstruction in pp collision events at $\sqrt{s} = 7$ TeV", *JINST* **7** (2012) P10002, `doi:10.1088/1748-0221/7/10/P10002`, `arXiv:1206.4071`.

[28] CMS Collaboration, "The CMS trigger system", *JINST* **12** (2017) P01020, `doi:10.1088/1748-0221/12/01/P01020`, `arXiv:1609.02366`.

[29] CMS Collaboration, "Performance of electron reconstruction and selection with the CMS detector in proton-proton collisions at $\sqrt{s} = 8$ TeV", *JINST* **10** (2015) P06005, `doi:10.1088/1748-0221/10/06/P06005`, `arXiv:1502.02701`.

[30] CMS Collaboration, "Jet energy scale and resolution in the CMS experiment in pp collisions at 8 TeV", *JINST* **12** (2017) P02014, `doi:10.1088/1748-0221/12/02/P02014`, `arXiv:1607.03663`.

[31] S. Frixione, P. Nason, and C. Oleari, "Matching NLO QCD computations with parton shower simulations: the POWHEG method", *JHEP* **11** (2007) 070, `doi:10.1088/1126-6708/2007/11/070`, `arXiv:0709.2092`.

[32] E. Bagnaschi, G. Degrassi, P. Slavich, and A. Vicini, "Higgs production via gluon fusion in the POWHEG approach in the SM and in the MSSM", *JHEP* **02** (2012) 088, `doi:10.1007/JHEP02(2012)088`, `arXiv:1111.2854`.

[33] P. Nason and C. Oleari, "NLO Higgs boson production via vector-boson fusion matched with shower in POWHEG", *JHEP* **02** (2010) 037, `doi:10.1007/JHEP02(2010)037`, `arXiv:0911.5299`.

[34] P. Nason, "A New method for combining NLO QCD with shower Monte Carlo algorithms", *JHEP* **11** (2004) 040, `doi:10.1088/1126-6708/2004/11/040`, `arXiv:hep-ph/0409146`.

[35] S. Alioli, P. Nason, C. Oleari, and E. Re, "A general framework for implementing NLO calculations in shower Monte Carlo programs: the POWHEG BOX", *JHEP* **06** (2010) 043, `doi:10.1007/JHEP06(2010)043`, `arXiv:1002.2581`.

[36] Y. Gao et al., "Spin determination of single-produced resonances at hadron colliders", *Phys. Rev. D* **81** (2010) 075022, `doi:10.1103/PhysRevD.81.075022`, `arXiv:1001.3396`.

[37] S. Bolognesi et al., "Spin and parity of a single-produced resonance at the LHC", *Phys. Rev. D* **86** (2012) 095031, `doi:10.1103/PhysRevD.86.095031`, `arXiv:1208.4018`.

[38] I. Anderson et al., "Constraining anomalous HVV interactions at proton and lepton colliders", *Phys. Rev. D* **89** (2014) 035007, `doi:10.1103/PhysRevD.89.035007`, `arXiv:1309.4819`.

[39] A. V. Gritsan, R. Roentsch, M. Schulze, and M. Xiao, "Constraining anomalous Higgs boson couplings to the heavy flavor fermions using matrix element techniques", *Phys. Rev. D* **94** (2016) 055023, `doi:10.1103/PhysRevD.94.055023`, `arXiv:1606.03107`.

[40] J. M. Campbell and R. K. Ellis, "MCFM for the Tevatron and the LHC", *Nucl. Phys. Proc. Suppl.* **205** (2010) 10, `doi:10.1016/j.nuclphysbps.2010.08.011`, `arXiv:1007.3492`.

[41] J. M. Campbell, R. K. Ellis, and C. Williams, "Vector boson pair production at the LHC", *JHEP* **07** (2011) 018, `doi:10.1007/JHEP07(2011)018`, `arXiv:1105.0020`.

[42] J. M. Campbell, R. K. Ellis, and C. Williams, "Bounding the Higgs width at the LHC using full analytic results for gg $\to$ e$^-$e$^+\mu^-\mu^+$", *JHEP* **04** (2014) 060, `doi:10.1007/JHEP04(2014)060`, `arXiv:1311.3589`.

[43] A. Ballestrero et al., "PHANTOM: a Monte Carlo event generator for six parton final states at high energy colliders", *Comput. Phys. Commun.* **180** (2009) 401, `doi:10.1016/j.cpc.2008.10.005`, `arXiv:0801.3359`.

[44] NNPDF Collaboration, "Parton distributions for the LHC run II", *JHEP* **04** (2015) 040, `doi:10.1007/JHEP04(2015)040`, `arXiv:1410.8849`.

[45] S. Catani and M. Grazzini, "An NNLO subtraction formalism in hadron collisions and its application to Higgs boson production at the LHC", *Phys. Rev. Lett.* **98** (2007) 222002, `doi:10.1103/PhysRevLett.98.222002`, `arXiv:hep-ph/0703012`.

[46] M. Grazzini, "NNLO predictions for the Higgs boson signal in the H $\to WW \to \ell\nu\ell\nu$ and H$\to ZZ \to 4\ell$ decay channels", *JHEP* **02** (2008) 043, `doi:10.1088/1126-6708/2008/02/043`, `arXiv:0801.3232`.

[47] M. Grazzini and H. Sargsyan, "Heavy-quark mass effects in Higgs boson production at the LHC", *JHEP* **09** (2013) 129, `doi:10.1007/JHEP09(2013)129`, `arXiv:1306.4581`.

[48] F. Caola, K. Melnikov, R. Roentsch, and L. Tancredi, "QCD corrections to ZZ production in gluon fusion at the LHC", *Phys. Rev. D* **92** (2015) 094028, `doi:10.1103/PhysRevD.92.094028`, `arXiv:1509.06734`.

[49] K. Melnikov and M. Dowling, "Production of two Z-bosons in gluon fusion in the heavy top quark approximation", *Phys. Lett. B* **744** (2015) 43, `doi:10.1016/j.physletb.2015.03.030`, `arXiv:1503.01274`.

[50] C. Anastasiou et al., "High precision determination of the gluon fusion Higgs boson cross-section at the LHC", *JHEP* **05** (2016) 058, `doi:10.1007/JHEP05(2016)058`, `arXiv:1602.00695`.

[51] D. de Florian et al., "Handbook of LHC Higgs Cross Sections: 4. Deciphering the Nature of the Higgs Sector", (2016). `arXiv:1610.07922`. CERN-2017-002-M.

[52] P. Nason and G. Zanderighi, "W^+W^-, WZ, and ZZ production in the POWHEG-BOX-V2", *Eur. Phys. J. C* **74** (2014) 2702, `doi:10.1140/epjc/s10052-013-2702-5`, `arXiv:1311.1365`.

[53] J. Alwall et al., "The automated computation of tree-level and next-to-leading order differential cross sections, and their matching to parton shower simulations", *JHEP* **07** (2014) 079, `doi:10.1007/JHEP07(2014)079`, `arXiv:1405.0301`.

[54] T. Sjöstrand, S. Mrenna, and P. Z. Skands, "A brief introduction to PYTHIA 8.1", *Comput. Phys. Commun.* **178** (2008) 852, `doi:10.1016/j.cpc.2008.01.036`, `arXiv:hep-ph/0710.3820`.

[55] M. Grazzini, S. Kallweit, D. Rathlev, and M. Wiesemann, "$W^\pm Z$ production at hadron colliders in NNLO QCD", *Phys. Lett. B* **761** (2016) 179, `doi:10.1016/j.physletb.2016.08.017`, `arXiv:1604.08576`.

[56] R. Frederix and S. Frixione, "Merging meets matching in MC@NLO", *JHEP* **12** (2012) 061, `doi:10.1007/JHEP12(2012)061`, `arXiv:1209.6215`.

[57] S. Frixione, P. Nason, and G. Ridolfi, "A positive-weight next-to-leading-order Monte Carlo for heavy flavour hadroproduction", *JHEP* **09** (2007) 126, `doi:10.1088/1126-6708/2007/09/126`, `arXiv:0707.3088`.

[58] CMS Collaboration, "Event generator tunes obtained from underlying event and multiparton scattering measurements", *Eur. Phys. J. C* **76** (2016) 155, `doi:10.1140/epjc/s10052-016-3988-x`, `arXiv:hep-ph/1512.00815`.

[59] S. Agostinelli et al., "GEANT4—a simulation toolkit", *Nucl. Instrum. Meth. A* **506** (2003) 250, `doi:10.1016/S0168-9002(03)01368-8`.

[60] CMS Collaboration, "Limits on the Higgs boson lifetime and width from its decay to four charged leptons", *Phys. Rev. D* **92** (2015) 072010, `doi:10.1103/PhysRevD.92.072010`, `arXiv:1507.06656`.

[61] M. Cacciari and G. P. Salam, "Pileup subtraction using jet areas", *Phys. Lett. B* **659** (2008) 119, `doi:10.1016/j.physletb.2007.09.077`, `arXiv:0707.1378`.

[62] M. Cacciari, G. P. Salam, and G. Soyez, "The catchment area of jets", *JHEP* **04** (2008) 005, `doi:10.1088/1126-6708/2008/04/005`, `arXiv:0802.1188`.

[63] CMS Collaboration, "Measurements of properties of the Higgs boson decaying into the four-lepton final state in pp collisions at $\sqrt{s} = 13$ TeV", *JHEP* **11** (2017) 047, `doi:10.1007/JHEP11(2017)047`, `arXiv:1706.09936`.

[64] R. Frühwirth, "Application of Kalman filtering to track and vertex fitting", *Nucl. Instrum. Meth. A* **262** (1987) 444, `doi:10.1016/0168-9002(87)90887-4`.

[65] CMS Collaboration, "Measurement of the inclusive W and Z production cross sections in pp collisions at $\sqrt{s} = 7\,\mathrm{TeV}$", *JHEP* **10** (2011) 132, `doi:10.1007/JHEP10(2011)132`, `arXiv:1107.4789`.

[66] CMS Collaboration, "Identification of b-quark jets with the CMS experiment", *JINST* **8** (2013) P04013, `doi:10.1088/1748-0221/8/04/P04013`, `arXiv:1211.4462`.

[67] CMS Collaboration, "Identification of b quark jets at the CMS experiment in the LHC Run 2", Technical Report CMS-PAS-BTV-15-001, CERN, Geneva, 2016.

[68] Particle Data Group, C. Patrignani et al., "Review of particle physics", *Chin. Phys. C* **40** (2016) 100001, `doi:10.1088/1674-1137/40/10/100001`.

[69] S. D. Ellis, C. K. Vermilion, and J. R. Walsh, "Recombination algorithms and jet substructure: Pruning as a tool for heavy particle searches", *Phys. Rev. D* **81** (2010) 094023, `doi:10.1103/PhysRevD.81.094023`, `arXiv:hep-ph/0912.0033`.

[70] J. M. Butterworth, A. R. Davison, M. Rubin, and G. P. Salam, "Jet substructure as a new Higgs search channel at the LHC", *Phys. Rev. Lett.* **100** (2008) 242001, `doi:10.1103/PhysRevLett.100.242001`, `arXiv:hep-ph/0802.2470`.

[71] J. M. Butterworth, A. R. Davison, M. Rubin, and G. P. Salam, "Maximizing boosted top identification by minimizing N-subjettiness", *JHEP* **02** (2012) 093, `doi:10.1007/JHEP02(2012)093`, `arXiv:hep-ph/1108.2701`.

[72] M. Grazzini, S. Kallweit, and D. Rathlev, "ZZ production at the LHC: Fiducial cross sections and distributions in NNLO QCD", *Phys. Lett. B* **750** (2015) 407, `doi:10.1016/j.physletb.2015.09.055`, `arXiv:1507.06257`.

[73] S. Gieseke, T. Kasprzik, and J. H. Kuehn, "Vector-boson pair production and electroweak corrections in HERWIG++", *Eur. Phys. J. C* **74** (2014) 2988, `doi:10.1140/epjc/s10052-014-2988-y`, `arXiv:1401.3964`.

[74] A. Manohar, P. Nason, G. P. Salam, and G. Zanderighi, "How bright is the proton? A precise determination of the photon parton distribution function", *Phys. Rev. Lett.* **117** (2016) 242002, `doi:10.1103/PhysRevLett.117.242002`, `arXiv:1607.04266`.

[75] J. Baglio, L. D. Ninh, and M. M. Weber, "Massive gauge boson pair production at the LHC: a next-to-leading order story", *Phys. Rev. D* **88** (2013) 113005, `doi:10.1103/PhysRevD.88.113005`, `arXiv:1307.4331`. [Erratum: `doi:10.1103/PhysRevD.94.099902`].

[76] S. Frixione et al., "Electroweak and QCD corrections to top-pair hadroproduction in association with heavy bosons", *JHEP* **06** (2015) 184, `doi:10.1007/JHEP06(2015)184`, `arXiv:1504.03446`.

[77] S. Frixione et al., "Weak corrections to Higgs hadroproduction in association with a top-quark pair", *JHEP* **09** (2014) 065, `doi:10.1007/JHEP09(2014)065`, `arXiv:1407.0823`.

[78] L. Landau, "On the energy loss of fast particles by ionization", *J. Phys. (USSR)* **8** (1944) 201.

[79] M. Bähr et al., "Herwig++ physics and manual", *Eur. Phys. J. C* **58** (2008) 639, `doi:10.1140/epjc/s10052-008-0798-9`, `arXiv:0803.0883`.

[80] T. Junk, "Confidence level computation for combining searches with small statistics", *Nucl. Instrum. Meth. A* **434** (1999) 435, `doi:10.1016/S0168-9002(99)00498-2`, `arXiv:hep-ex/9902006`.

[81] A. L. Read, "Presentation of search results: The CL$_\mathrm{s}$ technique", *J. Phys. G* **28** (2002) 2693, `doi:10.1088/0954-3899/28/10/313`.

[82] G. Cowan, K. Cranmer, E. Gross, and O. Vitells, "Asymptotic formulae for likelihood-based tests of new physics", *Eur. Phys. J. C* **71** (2011) 1554, `doi:10.1140/epjc/s10052-011-1554-0`, `arXiv:1007.1727`. [Erratum: `doi:10.1140/epjc/s10052-013-2501-z`].

A The CMS Collaboration

Yerevan Physics Institute, Yerevan, Armenia
A.M. Sirunyan, A. Tumasyan

Institut für Hochenergiephysik, Wien, Austria
W. Adam, F. Ambrogi, E. Asilar, T. Bergauer, J. Brandstetter, E. Brondolin, M. Dragicevic, J. Erö, A. Escalante Del Valle, M. Flechl, M. Friedl, R. Frühwirth[1], V.M. Ghete, J. Grossmann, J. Hrubec, M. Jeitler[1], A. König, N. Krammer, I. Krätschmer, D. Liko, T. Madlener, I. Mikulec, E. Pree, N. Rad, H. Rohringer, J. Schieck[1], R. Schöfbeck, M. Spanring, D. Spitzbart, A. Taurok, W. Waltenberger, J. Wittmann, C.-E. Wulz[1], M. Zarucki

Institute for Nuclear Problems, Minsk, Belarus
V. Chekhovsky, V. Mossolov, J. Suarez Gonzalez

Universiteit Antwerpen, Antwerpen, Belgium
E.A. De Wolf, D. Di Croce, X. Janssen, J. Lauwers, M. Pieters, M. Van De Klundert, H. Van Haevermaet, P. Van Mechelen, N. Van Remortel

Vrije Universiteit Brussel, Brussel, Belgium
S. Abu Zeid, F. Blekman, J. D'Hondt, I. De Bruyn, J. De Clercq, K. Deroover, G. Flouris, D. Lontkovskyi, S. Lowette, I. Marchesini, S. Moortgat, L. Moreels, Q. Python, K. Skovpen, S. Tavernier, W. Van Doninck, P. Van Mulders, I. Van Parijs

Université Libre de Bruxelles, Bruxelles, Belgium
D. Beghin, B. Bilin, H. Brun, B. Clerbaux, G. De Lentdecker, H. Delannoy, B. Dorney, G. Fasanella, L. Favart, R. Goldouzian, A. Grebenyuk, A.K. Kalsi, T. Lenzi, J. Luetic, N. Postiau, T. Seva, E. Starling, C. Vander Velde, P. Vanlaer, D. Vannerom, R. Yonamine

Ghent University, Ghent, Belgium
T. Cornelis, D. Dobur, A. Fagot, M. Gul, I. Khvastunov[2], D. Poyraz, C. Roskas, D. Trocino, M. Tytgat, W. Verbeke, B. Vermassen, M. Vit, N. Zaganidis

Université Catholique de Louvain, Louvain-la-Neuve, Belgium
H. Bakhshiansohi, O. Bondu, S. Brochet, G. Bruno, C. Caputo, A. Caudron, P. David, S. De Visscher, C. Delaere, M. Delcourt, B. Francois, A. Giammanco, G. Krintiras, V. Lemaitre, A. Magitteri, A. Mertens, M. Musich, K. Piotrzkowski, L. Quertenmont, A. Saggio, M. Vidal Marono, S. Wertz, J. Zobec

Centro Brasileiro de Pesquisas Fisicas, Rio de Janeiro, Brazil
W.L. Aldá Júnior, F.L. Alves, G.A. Alves, L. Brito, G. Correia Silva, C. Hensel, A. Moraes, M.E. Pol, P. Rebello Teles

Universidade do Estado do Rio de Janeiro, Rio de Janeiro, Brazil
E. Belchior Batista Das Chagas, W. Carvalho, J. Chinellato[3], E. Coelho, E.M. Da Costa, G.G. Da Silveira[4], D. De Jesus Damiao, S. Fonseca De Souza, H. Malbouisson, M. Medina Jaime[5], M. Melo De Almeida, C. Mora Herrera, L. Mundim, H. Nogima, L.J. Sanchez Rosas, A. Santoro, A. Sznajder, M. Thiel, E.J. Tonelli Manganote[3], F. Torres Da Silva De Araujo, A. Vilela Pereira

Universidade Estadual Paulista [a], Universidade Federal do ABC [b], São Paulo, Brazil
S. Ahuja[a], C.A. Bernardes[a], L. Calligaris[a], T.R. Fernandez Perez Tomei[a], E.M. Gregores[b], P.G. Mercadante[b], S.F. Novaes[a], Sandra S. Padula[a], D. Romero Abad[b], J.C. Ruiz Vargas[a]

Institute for Nuclear Research and Nuclear Energy, Bulgarian Academy of Sciences, Sofia, Bulgaria
A. Aleksandrov, R. Hadjiiska, P. Iaydjiev, A. Marinov, M. Misheva, M. Rodozov, M. Shopova, G. Sultanov

University of Sofia, Sofia, Bulgaria
A. Dimitrov, L. Litov, B. Pavlov, P. Petkov

Beihang University, Beijing, China
W. Fang[6], X. Gao[6], L. Yuan

Institute of High Energy Physics, Beijing, China
M. Ahmad, J.G. Bian, G.M. Chen, H.S. Chen, M. Chen, Y. Chen, C.H. Jiang, D. Leggat, H. Liao, Z. Liu, F. Romeo, S.M. Shaheen, A. Spiezia, J. Tao, C. Wang, Z. Wang, E. Yazgan, H. Zhang, J. Zhao

State Key Laboratory of Nuclear Physics and Technology, Peking University, Beijing, China
Y. Ban, G. Chen, J. Li, Q. Li, S. Liu, Y. Mao, S.J. Qian, D. Wang, Z. Xu

Tsinghua University, Beijing, China
Y. Wang

Universidad de Los Andes, Bogota, Colombia
C. Avila, A. Cabrera, C.A. Carrillo Montoya, L.F. Chaparro Sierra, C. Florez, C.F. González Hernández, M.A. Segura Delgado

University of Split, Faculty of Electrical Engineering, Mechanical Engineering and Naval Architecture, Split, Croatia
B. Courbon, N. Godinovic, D. Lelas, I. Puljak, P.M. Ribeiro Cipriano, T. Sculac

University of Split, Faculty of Science, Split, Croatia
Z. Antunovic, M. Kovac

Institute Rudjer Boskovic, Zagreb, Croatia
V. Brigljevic, D. Ferencek, K. Kadija, B. Mesic, A. Starodumov[7], T. Susa

University of Cyprus, Nicosia, Cyprus
M.W. Ather, A. Attikis, G. Mavromanolakis, J. Mousa, C. Nicolaou, F. Ptochos, P.A. Razis, H. Rykaczewski

Charles University, Prague, Czech Republic
M. Finger[8], M. Finger Jr.[8]

Universidad San Francisco de Quito, Quito, Ecuador
E. Carrera Jarrin

Academy of Scientific Research and Technology of the Arab Republic of Egypt, Egyptian Network of High Energy Physics, Cairo, Egypt
H. Abdalla[9], E. El-khateeb[10], M.A. Mahmoud[11,12]

National Institute of Chemical Physics and Biophysics, Tallinn, Estonia
S. Bhowmik, R.K. Dewanjee, M. Kadastik, L. Perrini, M. Raidal, C. Veelken

Department of Physics, University of Helsinki, Helsinki, Finland
P. Eerola, H. Kirschenmann, J. Pekkanen, M. Voutilainen

Helsinki Institute of Physics, Helsinki, Finland
J. Havukainen, J.K. Heikkilä, T. Järvinen, V. Karimäki, R. Kinnunen, T. Lampén, K. Lassila-Perini, S. Laurila, S. Lehti, T. Lindén, P. Luukka, T. Mäenpää, H. Siikonen, E. Tuominen, J. Tuominiemi

Lappeenranta University of Technology, Lappeenranta, Finland
T. Tuuva

IRFU, CEA, Université Paris-Saclay, Gif-sur-Yvette, France
M. Besancon, F. Couderc, M. Dejardin, D. Denegri, J.L. Faure, F. Ferri, S. Ganjour, S. Ghosh, A. Givernaud, P. Gras, G. Hamel de Monchenault, P. Jarry, C. Leloup, E. Locci, M. Machet, J. Malcles, G. Negro, J. Rander, A. Rosowsky, M.Ö. Sahin, M. Titov

Laboratoire Leprince-Ringuet, Ecole polytechnique, CNRS/IN2P3, Université Paris-Saclay, Palaiseau, France
A. Abdulsalam[13], C. Amendola, I. Antropov, S. Baffioni, F. Beaudette, P. Busson, L. Cadamuro, C. Charlot, R. Granier de Cassagnac, M. Jo, I. Kucher, S. Lisniak, A. Lobanov, J. Martin Blanco, M. Nguyen, C. Ochando, G. Ortona, P. Paganini, P. Pigard, R. Salerno, J.B. Sauvan, Y. Sirois, A.G. Stahl Leiton, Y. Yilmaz, A. Zabi, A. Zghiche

Université de Strasbourg, CNRS, IPHC UMR 7178, F-67000 Strasbourg, France
J.-L. Agram[14], J. Andrea, D. Bloch, J.-M. Brom, M. Buttignol, E.C. Chabert, C. Collard, E. Conte[14], X. Coubez, F. Drouhin[14], J.-C. Fontaine[14], D. Gelé, U. Goerlach, M. Jansová, P. Juillot, A.-C. Le Bihan, N. Tonon, P. Van Hove

Centre de Calcul de l'Institut National de Physique Nucleaire et de Physique des Particules, CNRS/IN2P3, Villeurbanne, France
S. Gadrat

Université de Lyon, Université Claude Bernard Lyon 1, CNRS-IN2P3, Institut de Physique Nucléaire de Lyon, Villeurbanne, France
S. Beauceron, C. Bernet, G. Boudoul, N. Chanon, R. Chierici, D. Contardo, P. Depasse, H. El Mamouni, J. Fay, L. Finco, S. Gascon, M. Gouzevitch, G. Grenier, B. Ille, F. Lagarde, I.B. Laktineh, H. Lattaud, M. Lethuillier, L. Mirabito, A.L. Pequegnot, S. Perries, A. Popov[15], V. Sordini, M. Vander Donckt, S. Viret, S. Zhang

Georgian Technical University, Tbilisi, Georgia
A. Khvedelidze[8]

Tbilisi State University, Tbilisi, Georgia
Z. Tsamalaidze[8]

RWTH Aachen University, I. Physikalisches Institut, Aachen, Germany
C. Autermann, L. Feld, M.K. Kiesel, K. Klein, M. Lipinski, M. Preuten, M.P. Rauch, C. Schomakers, J. Schulz, M. Teroerde, B. Wittmer, V. Zhukov[15]

RWTH Aachen University, III. Physikalisches Institut A, Aachen, Germany
A. Albert, D. Duchardt, M. Endres, M. Erdmann, S. Erdweg, T. Esch, R. Fischer, A. Güth, T. Hebbeker, C. Heidemann, K. Hoepfner, S. Knutzen, M. Merschmeyer, A. Meyer, P. Millet, S. Mukherjee, T. Pook, M. Radziej, H. Reithler, M. Rieger, F. Scheuch, D. Teyssier, S. Thüer

RWTH Aachen University, III. Physikalisches Institut B, Aachen, Germany
G. Flügge, B. Kargoll, T. Kress, A. Künsken, T. Müller, A. Nehrkorn, A. Nowack, C. Pistone, O. Pooth, A. Stahl[16]

Deutsches Elektronen-Synchrotron, Hamburg, Germany
M. Aldaya Martin, T. Arndt, C. Asawatangtrakuldee, K. Beernaert, O. Behnke, U. Behrens, A. Bermúdez Martínez, A.A. Bin Anuar, K. Borras[17], V. Botta, A. Campbell, P. Connor, C. Contreras-Campana, F. Costanza, V. Danilov, A. De Wit, C. Diez Pardos, D. Domínguez Damiani, G. Eckerlin, D. Eckstein, T. Eichhorn, E. Eren, E. Gallo[18], J. Garay Garcia, A. Geiser, J.M. Grados Luyando, A. Grohsjean, P. Gunnellini, M. Guthoff, A. Harb, J. Hauk, M. Hempel[19], H. Jung, M. Kasemann, J. Keaveney, C. Kleinwort, J. Knolle, I. Korol, D. Krücker, W. Lange, A. Lelek, T. Lenz, K. Lipka, W. Lohmann[19], R. Mankel, I.-A. Melzer-Pellmann, A.B. Meyer, M. Meyer, M. Missiroli, G. Mittag, J. Mnich, A. Mussgiller, D. Pitzl, A. Raspereza, M. Savitskyi, P. Saxena, R. Shevchenko, N. Stefaniuk, H. Tholen, G.P. Van Onsem, R. Walsh, Y. Wen, K. Wichmann, C. Wissing, O. Zenaiev

University of Hamburg, Hamburg, Germany
R. Aggleton, S. Bein, V. Blobel, M. Centis Vignali, T. Dreyer, E. Garutti, D. Gonzalez, J. Haller, A. Hinzmann, M. Hoffmann, A. Karavdina, G. Kasieczka, R. Klanner, R. Kogler, N. Kovalchuk, S. Kurz, D. Marconi, J. Multhaup, M. Niedziela, D. Nowatschin, T. Peiffer, A. Perieanu, A. Reimers, C. Scharf, P. Schleper, A. Schmidt, S. Schumann, J. Schwandt, J. Sonneveld, H. Stadie, G. Steinbrück, F.M. Stober, M. Stöver, D. Troendle, E. Usai, A. Vanhoefer, B. Vormwald

Institut für Experimentelle Teilchenphysik, Karlsruhe, Germany
M. Akbiyik, C. Barth, M. Baselga, S. Baur, E. Butz, R. Caspart, T. Chwalek, F. Colombo, W. De Boer, A. Dierlamm, N. Faltermann, B. Freund, R. Friese, M. Giffels, M.A. Harrendorf, F. Hartmann[16], S.M. Heindl, U. Husemann, F. Kassel[16], S. Kudella, H. Mildner, M.U. Mozer, Th. Müller, M. Plagge, G. Quast, K. Rabbertz, M. Schröder, I. Shvetsov, G. Sieber, H.J. Simonis, R. Ulrich, S. Wayand, M. Weber, T. Weiler, S. Williamson, C. Wöhrmann, R. Wolf

Institute of Nuclear and Particle Physics (INPP), NCSR Demokritos, Aghia Paraskevi, Greece
G. Anagnostou, G. Daskalakis, T. Geralis, A. Kyriakis, D. Loukas, I. Topsis-Giotis

National and Kapodistrian University of Athens, Athens, Greece
G. Karathanasis, S. Kesisoglou, A. Panagiotou, N. Saoulidou, E. Tziaferi

National Technical University of Athens, Athens, Greece
K. Kousouris, I. Papakrivopoulos

University of Ioánnina, Ioánnina, Greece
I. Evangelou, C. Foudas, P. Gianneios, P. Katsoulis, P. Kokkas, S. Mallios, N. Manthos, I. Papadopoulos, E. Paradas, J. Strologas, F.A. Triantis, D. Tsitsonis

MTA-ELTE Lendület CMS Particle and Nuclear Physics Group, Eötvös Loránd University, Budapest, Hungary
M. Csanad, N. Filipovic, G. Pasztor, O. Surányi, G.I. Veres[20]

Wigner Research Centre for Physics, Budapest, Hungary
G. Bencze, C. Hajdu, D. Horvath[21], Á. Hunyadi, F. Sikler, T.Á. Vámi, V. Veszpremi, G. Vesztergombi[20]

Institute of Nuclear Research ATOMKI, Debrecen, Hungary
N. Beni, S. Czellar, J. Karancsi[22], A. Makovec, J. Molnar, Z. Szillasi

Institute of Physics, University of Debrecen, Debrecen, Hungary
M. Bartók[20], P. Raics, Z.L. Trocsanyi, B. Ujvari

Indian Institute of Science (IISc), Bangalore, India
S. Choudhury, J.R. Komaragiri

National Institute of Science Education and Research, Bhubaneswar, India
S. Bahinipati[23], P. Mal, K. Mandal, A. Nayak[24], D.K. Sahoo[23], S.K. Swain

Panjab University, Chandigarh, India
S. Bansal, S.B. Beri, V. Bhatnagar, S. Chauhan, R. Chawla, N. Dhingra, R. Gupta, A. Kaur, M. Kaur, S. Kaur, R. Kumar, P. Kumari, M. Lohan, A. Mehta, S. Sharma, J.B. Singh, G. Walia

University of Delhi, Delhi, India
A. Bhardwaj, B.C. Choudhary, R.B. Garg, S. Keshri, A. Kumar, Ashok Kumar, S. Malhotra, M. Naimuddin, K. Ranjan, Aashaq Shah, R. Sharma

Saha Institute of Nuclear Physics, HBNI, Kolkata, India
R. Bhardwaj[25], R. Bhattacharya, S. Bhattacharya, U. Bhawandeep[25], D. Bhowmik, S. Dey, S. Dutt[25], S. Dutta, S. Ghosh, N. Majumdar, K. Mondal, S. Mukhopadhyay, S. Nandan, A. Purohit, P.K. Rout, A. Roy, S. Roy Chowdhury, S. Sarkar, M. Sharan, B. Singh, S. Thakur[25]

Indian Institute of Technology Madras, Madras, India
P.K. Behera

Bhabha Atomic Research Centre, Mumbai, India
R. Chudasama, D. Dutta, V. Jha, V. Kumar, A.K. Mohanty[16], P.K. Netrakanti, L.M. Pant, P. Shukla, A. Topkar

Tata Institute of Fundamental Research-A, Mumbai, India
T. Aziz, S. Dugad, B. Mahakud, S. Mitra, G.B. Mohanty, N. Sur, B. Sutar

Tata Institute of Fundamental Research-B, Mumbai, India
S. Banerjee, S. Bhattacharya, S. Chatterjee, P. Das, M. Guchait, Sa. Jain, S. Kumar, M. Maity[26], G. Majumder, K. Mazumdar, N. Sahoo, T. Sarkar[26], N. Wickramage[27]

Indian Institute of Science Education and Research (IISER), Pune, India
S. Chauhan, S. Dube, V. Hegde, A. Kapoor, K. Kothekar, S. Pandey, A. Rane, S. Sharma

Institute for Research in Fundamental Sciences (IPM), Tehran, Iran
S. Chenarani[28], E. Eskandari Tadavani, S.M. Etesami[28], M. Khakzad, M. Mohammadi Najafabadi, M. Naseri, S. Paktinat Mehdiabadi[29], F. Rezaei Hosseinabadi, B. Safarzadeh[30], M. Zeinali

University College Dublin, Dublin, Ireland
M. Felcini, M. Grunewald

INFN Sezione di Bari [a], Università di Bari [b], Politecnico di Bari [c], Bari, Italy
M. Abbrescia[a,b], C. Calabria[a,b], A. Colaleo[a], D. Creanza[a,c], L. Cristella[a,b], N. De Filippis[a,c], M. De Palma[a,b], A. Di Florio[a,b], F. Errico[a,b], L. Fiore[a], A. Gelmi[a,b], G. Iaselli[a,c], S. Lezki[a,b], G. Maggi[a,c], M. Maggi[a], B. Marangelli[a,b], G. Miniello[a,b], S. My[a,b], S. Nuzzo[a,b], A. Pompili[a,b], G. Pugliese[a,c], R. Radogna[a], A. Ranieri[a], G. Selvaggi[a,b], A. Sharma[a], L. Silvestris[a,16], R. Venditti[a], P. Verwilligen[a], G. Zito[a]

INFN Sezione di Bologna [a], Università di Bologna [b], Bologna, Italy
G. Abbiendi[a], C. Battilana[a,b], D. Bonacorsi[a,b], L. Borgonovi[a,b], S. Braibant-Giacomelli[a,b], R. Campanini[a,b], P. Capiluppi[a,b], A. Castro[a,b], F.R. Cavallo[a], S.S. Chhibra[a,b], G. Codispoti[a,b], M. Cuffiani[a,b], G.M. Dallavalle[a], F. Fabbri[a], A. Fanfani[a,b], D. Fasanella[a,b], P. Giacomelli[a],

C. Grandi[a], L. Guiducci[a,b], S. Marcellini[a], G. Masetti[a], A. Montanari[a], F.L. Navarria[a,b], F. Odorici[a], A. Perrotta[a], A.M. Rossi[a,b], T. Rovelli[a,b], G.P. Siroli[a,b], N. Tosi[a]

INFN Sezione di Catania [a]**, Università di Catania** [b]**, Catania, Italy**
S. Albergo[a,b], S. Costa[a,b], A. Di Mattia[a], F. Giordano[a,b], R. Potenza[a,b], A. Tricomi[a,b], C. Tuve[a,b]

INFN Sezione di Firenze [a]**, Università di Firenze** [b]**, Firenze, Italy**
G. Barbagli[a], K. Chatterjee[a,b], V. Ciulli[a,b], C. Civinini[a], R. D'Alessandro[a,b], E. Focardi[a,b], G. Latino, P. Lenzi[a,b], M. Meschini[a], S. Paoletti[a], L. Russo[a,31], G. Sguazzoni[a], D. Strom[a], L. Viliani[a]

INFN Laboratori Nazionali di Frascati, Frascati, Italy
L. Benussi, S. Bianco, F. Fabbri, D. Piccolo, F. Primavera[16]

INFN Sezione di Genova [a]**, Università di Genova** [b]**, Genova, Italy**
V. Calvelli[a,b], F. Ferro[a], F. Ravera[a,b], E. Robutti[a], S. Tosi[a,b]

INFN Sezione di Milano-Bicocca [a]**, Università di Milano-Bicocca** [b]**, Milano, Italy**
A. Benaglia[a], A. Beschi[b], L. Brianza[a,b], F. Brivio[a,b], V. Ciriolo[a,b,16], M.E. Dinardo[a,b], S. Fiorendi[a,b], S. Gennai[a], A. Ghezzi[a,b], P. Govoni[a,b], M. Malberti[a,b], S. Malvezzi[a], R.A. Manzoni[a,b], D. Menasce[a], L. Moroni[a], M. Paganoni[a,b], K. Pauwels[a,b], D. Pedrini[a], S. Pigazzini[a,b,32], S. Ragazzi[a,b], T. Tabarelli de Fatis[a,b]

INFN Sezione di Napoli [a]**, Università di Napoli 'Federico II'** [b]**, Napoli, Italy, Università della Basilicata** [c]**, Potenza, Italy, Università G. Marconi** [d]**, Roma, Italy**
S. Buontempo[a], N. Cavallo[a,c], S. Di Guida[a,d,16], F. Fabozzi[a,c], F. Fienga[a,b], G. Galati[a,b], A.O.M. Iorio[a,b], W.A. Khan[a], L. Lista[a], S. Meola[a,d,16], P. Paolucci[a,16], C. Sciacca[a,b], F. Thyssen[a], E. Voevodina[a,b]

INFN Sezione di Padova [a]**, Università di Padova** [b]**, Padova, Italy, Università di Trento** [c]**, Trento, Italy**
P. Azzi[a], N. Bacchetta[a], L. Benato[a,b], D. Bisello[a,b], A. Boletti[a,b], R. Carlin[a,b], A. Carvalho Antunes De Oliveira[a,b], P. Checchia[a], M. Dall'Osso[a,b], P. De Castro Manzano[a], T. Dorigo[a], U. Dosselli[a], F. Gasparini[a,b], U. Gasparini[a,b], A. Gozzelino[a], S. Lacaprara[a], P. Lujan, M. Margoni[a,b], A.T. Meneguzzo[a,b], N. Pozzobon[a,b], P. Ronchese[a,b], R. Rossin[a,b], A. Tiko, E. Torassa[a], M. Zanetti[a,b], P. Zotto[a,b], G. Zumerle[a,b]

INFN Sezione di Pavia [a]**, Università di Pavia** [b]**, Pavia, Italy**
A. Braghieri[a], A. Magnani[a], P. Montagna[a,b], S.P. Ratti[a,b], V. Re[a], M. Ressegotti[a,b], C. Riccardi[a,b], P. Salvini[a], I. Vai[a,b], P. Vitulo[a,b]

INFN Sezione di Perugia [a]**, Università di Perugia** [b]**, Perugia, Italy**
L. Alunni Solestizi[a,b], M. Biasini[a,b], G.M. Bilei[a], C. Cecchi[a,b], D. Ciangottini[a,b], L. Fanò[a,b], P. Lariccia[a,b], R. Leonardi[a,b], E. Manoni[a], G. Mantovani[a,b], V. Mariani[a,b], M. Menichelli[a], A. Rossi[a,b], A. Santocchia[a,b], D. Spiga[a]

INFN Sezione di Pisa [a]**, Università di Pisa** [b]**, Scuola Normale Superiore di Pisa** [c]**, Pisa, Italy**
K. Androsov[a], P. Azzurri[a,16], G. Bagliesi[a], L. Bianchini[a], T. Boccali[a], L. Borrello, R. Castaldi[a], M.A. Ciocci[a,b], R. Dell'Orso[a], G. Fedi[a], L. Giannini[a,c], A. Giassi[a], M.T. Grippo[a,31], F. Ligabue[a,c], T. Lomtadze[a], E. Manca[a,c], G. Mandorli[a,c], A. Messineo[a,b], F. Palla[a], A. Rizzi[a,b], P. Spagnolo[a], R. Tenchini[a], G. Tonelli[a,b], A. Venturi[a], P.G. Verdini[a]

INFN Sezione di Roma [a]**, Sapienza Università di Roma** [b]**, Rome, Italy**
L. Barone[a,b], F. Cavallari[a], M. Cipriani[a,b], N. Daci[a], D. Del Re[a,b], E. Di Marco[a,b], M. Diemoz[a],

S. Gelli[a,b], E. Longo[a,b], B. Marzocchi[a,b], P. Meridiani[a], G. Organtini[a,b], F. Pandolfi[a], R. Paramatti[a,b], F. Preiato[a,b], S. Rahatlou[a,b], C. Rovelli[a], F. Santanastasio[a,b]

INFN Sezione di Torino [a], Università di Torino [b], Torino, Italy, Università del Piemonte Orientale [c], Novara, Italy
N. Amapane[a,b], R. Arcidiacono[a,c], S. Argiro[a,b], M. Arneodo[a,c], N. Bartosik[a], R. Bellan[a,b], C. Biino[a], N. Cartiglia[a], R. Castello[a,b], F. Cenna[a,b], M. Costa[a,b], R. Covarelli[a,b], A. Degano[a,b], N. Demaria[a], B. Kiani[a,b], C. Mariotti[a], S. Maselli[a], E. Migliore[a,b], V. Monaco[a,b], E. Monteil[a,b], M. Monteno[a], M.M. Obertino[a,b], L. Pacher[a,b], N. Pastrone[a], M. Pelliccioni[a], G.L. Pinna Angioni[a,b], A. Romero[a,b], M. Ruspa[a,c], R. Sacchi[a,b], K. Shchelina[a,b], V. Sola[a], A. Solano[a,b], A. Staiano[a]

INFN Sezione di Trieste [a], Università di Trieste [b], Trieste, Italy
S. Belforte[a], M. Casarsa[a], F. Cossutti[a], G. Della Ricca[a,b], A. Zanetti[a]

Kyungpook National University
D.H. Kim, G.N. Kim, M.S. Kim, J. Lee, S. Lee, S.W. Lee, C.S. Moon, Y.D. Oh, S. Sekmen, D.C. Son, Y.C. Yang

Chonnam National University, Institute for Universe and Elementary Particles, Kwangju, Korea
H. Kim, D.H. Moon, G. Oh

Hanyang University, Seoul, Korea
J.A. Brochero Cifuentes, J. Goh, T.J. Kim

Korea University, Seoul, Korea
S. Cho, S. Choi, Y. Go, D. Gyun, S. Ha, B. Hong, Y. Jo, Y. Kim, K. Lee, K.S. Lee, S. Lee, J. Lim, S.K. Park, Y. Roh

Seoul National University, Seoul, Korea
J. Almond, J. Kim, J.S. Kim, H. Lee, K. Lee, K. Nam, S.B. Oh, B.C. Radburn-Smith, S.h. Seo, U.K. Yang, H.D. Yoo, G.B. Yu

University of Seoul, Seoul, Korea
H. Kim, J.H. Kim, J.S.H. Lee, I.C. Park

Sungkyunkwan University, Suwon, Korea
Y. Choi, C. Hwang, J. Lee, I. Yu

Vilnius University, Vilnius, Lithuania
V. Dudenas, A. Juodagalvis, J. Vaitkus

National Centre for Particle Physics, Universiti Malaya, Kuala Lumpur, Malaysia
I. Ahmed, Z.A. Ibrahim, M.A.B. Md Ali[33], F. Mohamad Idris[34], W.A.T. Wan Abdullah, M.N. Yusli, Z. Zolkapli

Centro de Investigacion y de Estudios Avanzados del IPN, Mexico City, Mexico
Duran-Osuna, M. C., H. Castilla-Valdez, E. De La Cruz-Burelo, Ramirez-Sanchez, G., I. Heredia-De La Cruz[35], Rabadan-Trejo, R. I., R. Lopez-Fernandez, J. Mejia Guisao, Reyes-Almanza, R, A. Sanchez-Hernandez

Universidad Iberoamericana, Mexico City, Mexico
S. Carrillo Moreno, C. Oropeza Barrera, F. Vazquez Valencia

Benemerita Universidad Autonoma de Puebla, Puebla, Mexico
J. Eysermans, I. Pedraza, H.A. Salazar Ibarguen, C. Uribe Estrada

Universidad Autónoma de San Luis Potosí, San Luis Potosí, Mexico
A. Morelos Pineda

University of Auckland, Auckland, New Zealand
D. Krofcheck

University of Canterbury, Christchurch, New Zealand
S. Bheesette, P.H. Butler

National Centre for Physics, Quaid-I-Azam University, Islamabad, Pakistan
A. Ahmad, M. Ahmad, Q. Hassan, H.R. Hoorani, A. Saddique, M.A. Shah, M. Shoaib, M. Waqas

National Centre for Nuclear Research, Swierk, Poland
H. Bialkowska, M. Bluj, B. Boimska, T. Frueboes, M. Górski, M. Kazana, K. Nawrocki, M. Szleper, P. Traczyk, P. Zalewski

Institute of Experimental Physics, Faculty of Physics, University of Warsaw, Warsaw, Poland
K. Bunkowski, A. Byszuk[36], K. Doroba, A. Kalinowski, M. Konecki, J. Krolikowski, M. Misiura, M. Olszewski, A. Pyskir, M. Walczak

Laboratório de Instrumentação e Física Experimental de Partículas, Lisboa, Portugal
P. Bargassa, C. Beirão Da Cruz E Silva, A. Di Francesco, P. Faccioli, B. Galinhas, M. Gallinaro, J. Hollar, N. Leonardo, L. Lloret Iglesias, M.V. Nemallapudi, J. Seixas, G. Strong, O. Toldaiev, D. Vadruccio, J. Varela

Joint Institute for Nuclear Research, Dubna, Russia
V. Alexakhin, A. Golunov, I. Golutvin, N. Gorbounov, I. Gorbunov, A. Kamenev, V. Karjavin, A. Lanev, A. Malakhov, V. Matveev[37,38], P. Moisenz, V. Palichik, V. Perelygin, M. Savina, S. Shmatov, S. Shulha, N. Skatchkov, V. Smirnov, A. Zarubin

Petersburg Nuclear Physics Institute, Gatchina (St. Petersburg), Russia
Y. Ivanov, V. Kim[39], E. Kuznetsova[40], P. Levchenko, V. Murzin, V. Oreshkin, I. Smirnov, D. Sosnov, V. Sulimov, L. Uvarov, S. Vavilov, A. Vorobyev

Institute for Nuclear Research, Moscow, Russia
Yu. Andreev, A. Dermenev, S. Gninenko, N. Golubev, A. Karneyeu, M. Kirsanov, N. Krasnikov, A. Pashenkov, D. Tlisov, A. Toropin

Institute for Theoretical and Experimental Physics, Moscow, Russia
V. Epshteyn, V. Gavrilov, N. Lychkovskaya, V. Popov, I. Pozdnyakov, G. Safronov, A. Spiridonov, A. Stepennov, V. Stolin, M. Toms, E. Vlasov, A. Zhokin

Moscow Institute of Physics and Technology, Moscow, Russia
T. Aushev, A. Bylinkin[38]

National Research Nuclear University 'Moscow Engineering Physics Institute' (MEPhI), Moscow, Russia
R. Chistov[41], M. Danilov[41], P. Parygin, D. Philippov, S. Polikarpov, E. Tarkovskii

P.N. Lebedev Physical Institute, Moscow, Russia
V. Andreev, M. Azarkin[38], I. Dremin[38], M. Kirakosyan[38], S.V. Rusakov, A. Terkulov

Skobeltsyn Institute of Nuclear Physics, Lomonosov Moscow State University, Moscow, Russia
A. Baskakov, A. Belyaev, E. Boos, V. Bunichev, M. Dubinin[42], L. Dudko, A. Ershov, A. Gribushin, V. Klyukhin, O. Kodolova, I. Lokhtin, I. Miagkov, S. Obraztsov, S. Petrushanko, V. Savrin

Novosibirsk State University (NSU), Novosibirsk, Russia
V. Blinov[43], D. Shtol[43], Y. Skovpen[43]

State Research Center of Russian Federation, Institute for High Energy Physics of NRC &quot, Kurchatov Institute&quot, , Protvino, Russia
I. Azhgirey, I. Bayshev, S. Bitioukov, D. Elumakhov, A. Godizov, V. Kachanov, A. Kalinin, D. Konstantinov, P. Mandrik, V. Petrov, R. Ryutin, A. Sobol, S. Troshin, N. Tyurin, A. Uzunian, A. Volkov

National Research Tomsk Polytechnic University, Tomsk, Russia
A. Babaev

University of Belgrade, Faculty of Physics and Vinca Institute of Nuclear Sciences, Belgrade, Serbia
P. Adzic[44], P. Cirkovic, D. Devetak, M. Dordevic, J. Milosevic

Centro de Investigaciones Energéticas Medioambientales y Tecnológicas (CIEMAT), Madrid, Spain
J. Alcaraz Maestre, A. Álvarez Fernández, I. Bachiller, M. Barrio Luna, M. Cerrada, N. Colino, B. De La Cruz, A. Delgado Peris, C. Fernandez Bedoya, J.P. Fernández Ramos, J. Flix, M.C. Fouz, O. Gonzalez Lopez, S. Goy Lopez, J.M. Hernandez, M.I. Josa, D. Moran, A. Pérez-Calero Yzquierdo, J. Puerta Pelayo, I. Redondo, L. Romero, M.S. Soares, A. Triossi

Universidad Autónoma de Madrid, Madrid, Spain
C. Albajar, J.F. de Trocóniz

Universidad de Oviedo, Oviedo, Spain
J. Cuevas, C. Erice, J. Fernandez Menendez, S. Folgueras, I. Gonzalez Caballero, J.R. González Fernández, E. Palencia Cortezon, S. Sanchez Cruz, P. Vischia, J.M. Vizan Garcia

Instituto de Física de Cantabria (IFCA), CSIC-Universidad de Cantabria, Santander, Spain
I.J. Cabrillo, A. Calderon, B. Chazin Quero, J. Duarte Campderros, M. Fernandez, P.J. Fernández Manteca, A. García Alonso, J. Garcia-Ferrero, G. Gomez, A. Lopez Virto, J. Marco, C. Martinez Rivero, P. Martinez Ruiz del Arbol, F. Matorras, J. Piedra Gomez, C. Prieels, T. Rodrigo, A. Ruiz-Jimeno, L. Scodellaro, N. Trevisani, I. Vila, R. Vilar Cortabitarte

CERN, European Organization for Nuclear Research, Geneva, Switzerland
D. Abbaneo, B. Akgun, E. Auffray, P. Baillon, A.H. Ball, D. Barney, J. Bendavid, M. Bianco, A. Bocci, C. Botta, T. Camporesi, M. Cepeda, G. Cerminara, E. Chapon, Y. Chen, D. d'Enterria, A. Dabrowski, V. Daponte, A. David, M. De Gruttola, A. De Roeck, N. Deelen, M. Dobson, T. du Pree, M. Dünser, N. Dupont, A. Elliott-Peisert, P. Everaerts, F. Fallavollita[45], G. Franzoni, J. Fulcher, W. Funk, D. Gigi, A. Gilbert, K. Gill, F. Glege, D. Gulhan, J. Hegeman, V. Innocente, A. Jafari, P. Janot, O. Karacheban[19], J. Kieseler, V. Knünz, A. Kornmayer, M. Krammer[1], C. Lange, P. Lecoq, C. Lourenço, M.T. Lucchini, L. Malgeri, M. Mannelli, A. Martelli, F. Meijers, J.A. Merlin, S. Mersi, E. Meschi, P. Milenovic[46], F. Moortgat, M. Mulders, H. Neugebauer, J. Ngadiuba, S. Orfanelli, L. Orsini, F. Pantaleo[16], L. Pape, E. Perez, M. Peruzzi, A. Petrilli, G. Petrucciani, A. Pfeiffer, M. Pierini, F.M. Pitters, D. Rabady, A. Racz, T. Reis, G. Rolandi[47], M. Rovere, H. Sakulin, C. Schäfer, C. Schwick, M. Seidel, M. Selvaggi, A. Sharma, P. Silva,

P. Sphicas[48], A. Stakia, J. Steggemann, M. Stoye, M. Tosi, D. Treille, A. Tsirou, V. Veckalns[49], M. Verweij, W.D. Zeuner

Paul Scherrer Institut, Villigen, Switzerland
W. Bertl[†], L. Caminada[50], K. Deiters, W. Erdmann, R. Horisberger, Q. Ingram, H.C. Kaestli, D. Kotlinski, U. Langenegger, T. Rohe, S.A. Wiederkehr

ETH Zurich - Institute for Particle Physics and Astrophysics (IPA), Zurich, Switzerland
M. Backhaus, L. Bäni, P. Berger, B. Casal, N. Chernyavskaya, G. Dissertori, M. Dittmar, M. Donegà, C. Dorfer, C. Grab, C. Heidegger, D. Hits, J. Hoss, T. Klijnsma, W. Lustermann, M. Marionneau, M.T. Meinhard, D. Meister, F. Micheli, P. Musella, F. Nessi-Tedaldi, J. Pata, F. Pauss, G. Perrin, L. Perrozzi, M. Quittnat, M. Reichmann, D. Ruini, D.A. Sanz Becerra, M. Schönenberger, L. Shchutska, V.R. Tavolaro, K. Theofilatos, M.L. Vesterbacka Olsson, R. Wallny, D.H. Zhu

Universität Zürich, Zurich, Switzerland
T.K. Aarrestad, C. Amsler[51], D. Brzhechko, M.F. Canelli, A. De Cosa, R. Del Burgo, S. Donato, C. Galloni, T. Hreus, B. Kilminster, I. Neutelings, D. Pinna, G. Rauco, P. Robmann, D. Salerno, K. Schweiger, C. Seitz, Y. Takahashi, A. Zucchetta

National Central University, Chung-Li, Taiwan
V. Candelise, Y.H. Chang, K.y. Cheng, T.H. Doan, Sh. Jain, R. Khurana, C.M. Kuo, W. Lin, A. Pozdnyakov, S.S. Yu

National Taiwan University (NTU), Taipei, Taiwan
P. Chang, Y. Chao, K.F. Chen, P.H. Chen, F. Fiori, W.-S. Hou, Y. Hsiung, Arun Kumar, Y.F. Liu, R.-S. Lu, E. Paganis, A. Psallidas, A. Steen, J.f. Tsai

Chulalongkorn University, Faculty of Science, Department of Physics, Bangkok, Thailand
B. Asavapibhop, K. Kovitanggoon, G. Singh, N. Srimanobhas

Çukurova University, Physics Department, Science and Art Faculty, Adana, Turkey
A. Bat, F. Boran, S. Cerci[52], S. Damarseckin, Z.S. Demiroglu, C. Dozen, I. Dumanoglu, S. Girgis, G. Gokbulut, Y. Guler, I. Hos[53], E.E. Kangal[54], O. Kara, U. Kiminsu, M. Oglakci, G. Onengut, K. Ozdemir[55], D. Sunar Cerci[52], B. Tali[52], U.G. Tok, H. Topakli[56], S. Turkcapar, I.S. Zorbakir, C. Zorbilmez

Middle East Technical University, Physics Department, Ankara, Turkey
G. Karapinar[57], K. Ocalan[58], M. Yalvac, M. Zeyrek

Bogazici University, Istanbul, Turkey
E. Gülmez, M. Kaya[59], O. Kaya[60], S. Tekten, E.A. Yetkin[61]

Istanbul Technical University, Istanbul, Turkey
M.N. Agaras, S. Atay, A. Cakir, K. Cankocak, Y. Komurcu

Institute for Scintillation Materials of National Academy of Science of Ukraine, Kharkov, Ukraine
B. Grynyov

National Scientific Center, Kharkov Institute of Physics and Technology, Kharkov, Ukraine
L. Levchuk

University of Bristol, Bristol, United Kingdom
F. Ball, L. Beck, J.J. Brooke, D. Burns, E. Clement, D. Cussans, O. Davignon, H. Flacher,

J. Goldstein, G.P. Heath, H.F. Heath, L. Kreczko, D.M. Newbold[62], S. Paramesvaran, T. Sakuma, S. Seif El Nasr-storey, D. Smith, V.J. Smith

Rutherford Appleton Laboratory, Didcot, United Kingdom
K.W. Bell, A. Belyaev[63], C. Brew, R.M. Brown, D. Cieri, D.J.A. Cockerill, J.A. Coughlan, K. Harder, S. Harper, J. Linacre, E. Olaiya, D. Petyt, C.H. Shepherd-Themistocleous, A. Thea, I.R. Tomalin, T. Williams, W.J. Womersley

Imperial College, London, United Kingdom
G. Auzinger, R. Bainbridge, P. Bloch, J. Borg, S. Breeze, O. Buchmuller, A. Bundock, S. Casasso, D. Colling, L. Corpe, P. Dauncey, G. Davies, M. Della Negra, R. Di Maria, A. Elwood, Y. Haddad, G. Hall, G. Iles, T. James, M. Komm, R. Lane, C. Laner, L. Lyons, A.-M. Magnan, S. Malik, L. Mastrolorenzo, T. Matsushita, J. Nash[64], A. Nikitenko[7], V. Palladino, M. Pesaresi, A. Richards, A. Rose, E. Scott, C. Seez, A. Shtipliyski, T. Strebler, S. Summers, A. Tapper, K. Uchida, M. Vazquez Acosta[65], T. Virdee[16], N. Wardle, D. Winterbottom, J. Wright, S.C. Zenz

Brunel University, Uxbridge, United Kingdom
J.E. Cole, P.R. Hobson, A. Khan, P. Kyberd, A. Morton, I.D. Reid, L. Teodorescu, S. Zahid

Baylor University, Waco, USA
A. Borzou, K. Call, J. Dittmann, K. Hatakeyama, H. Liu, N. Pastika, C. Smith

Catholic University of America, Washington DC, USA
R. Bartek, A. Dominguez

The University of Alabama, Tuscaloosa, USA
A. Buccilli, S.I. Cooper, C. Henderson, P. Rumerio, C. West

Boston University, Boston, USA
D. Arcaro, A. Avetisyan, T. Bose, D. Gastler, D. Rankin, C. Richardson, J. Rohlf, L. Sulak, D. Zou

Brown University, Providence, USA
G. Benelli, D. Cutts, M. Hadley, J. Hakala, U. Heintz, J.M. Hogan[66], K.H.M. Kwok, E. Laird, G. Landsberg, J. Lee, Z. Mao, M. Narain, J. Pazzini, S. Piperov, S. Sagir, R. Syarif, D. Yu

University of California, Davis, Davis, USA
R. Band, C. Brainerd, R. Breedon, D. Burns, M. Calderon De La Barca Sanchez, M. Chertok, J. Conway, R. Conway, P.T. Cox, R. Erbacher, C. Flores, G. Funk, W. Ko, R. Lander, C. Mclean, M. Mulhearn, D. Pellett, J. Pilot, S. Shalhout, M. Shi, J. Smith, D. Stolp, D. Taylor, K. Tos, M. Tripathi, Z. Wang, F. Zhang

University of California, Los Angeles, USA
M. Bachtis, C. Bravo, R. Cousins, A. Dasgupta, A. Florent, J. Hauser, M. Ignatenko, N. Mccoll, S. Regnard, D. Saltzberg, C. Schnaible, V. Valuev

University of California, Riverside, Riverside, USA
E. Bouvier, K. Burt, R. Clare, J. Ellison, J.W. Gary, S.M.A. Ghiasi Shirazi, G. Hanson, G. Karapostoli, E. Kennedy, F. Lacroix, O.R. Long, M. Olmedo Negrete, M.I. Paneva, W. Si, L. Wang, H. Wei, S. Wimpenny, B. R. Yates

University of California, San Diego, La Jolla, USA
J.G. Branson, S. Cittolin, M. Derdzinski, R. Gerosa, D. Gilbert, B. Hashemi, A. Holzner, D. Klein, G. Kole, V. Krutelyov, J. Letts, M. Masciovecchio, D. Olivito, S. Padhi, M. Pieri, M. Sani, V. Sharma, S. Simon, M. Tadel, A. Vartak, S. Wasserbaech[67], J. Wood, F. Würthwein, A. Yagil, G. Zevi Della Porta

University of California, Santa Barbara - Department of Physics, Santa Barbara, USA
N. Amin, R. Bhandari, J. Bradmiller-Feld, C. Campagnari, M. Citron, A. Dishaw, V. Dutta, M. Franco Sevilla, L. Gouskos, R. Heller, J. Incandela, A. Ovcharova, H. Qu, J. Richman, D. Stuart, I. Suarez, J. Yoo

California Institute of Technology, Pasadena, USA
D. Anderson, A. Bornheim, J. Bunn, J.M. Lawhorn, H.B. Newman, T. Q. Nguyen, C. Pena, M. Spiropulu, J.R. Vlimant, R. Wilkinson, S. Xie, Z. Zhang, R.Y. Zhu

Carnegie Mellon University, Pittsburgh, USA
M.B. Andrews, T. Ferguson, T. Mudholkar, M. Paulini, J. Russ, M. Sun, H. Vogel, I. Vorobiev, M. Weinberg

University of Colorado Boulder, Boulder, USA
J.P. Cumalat, W.T. Ford, F. Jensen, A. Johnson, M. Krohn, S. Leontsinis, E. MacDonald, T. Mulholland, K. Stenson, K.A. Ulmer, S.R. Wagner

Cornell University, Ithaca, USA
J. Alexander, J. Chaves, Y. Cheng, J. Chu, A. Datta, K. Mcdermott, N. Mirman, J.R. Patterson, D. Quach, A. Rinkevicius, A. Ryd, L. Skinnari, L. Soffi, S.M. Tan, Z. Tao, J. Thom, J. Tucker, P. Wittich, M. Zientek

Fermi National Accelerator Laboratory, Batavia, USA
S. Abdullin, M. Albrow, M. Alyari, G. Apollinari, A. Apresyan, A. Apyan, S. Banerjee, L.A.T. Bauerdick, A. Beretvas, J. Berryhill, P.C. Bhat, G. Bolla[†], K. Burkett, J.N. Butler, A. Canepa, G.B. Cerati, H.W.K. Cheung, F. Chlebana, M. Cremonesi, J. Duarte, V.D. Elvira, J. Freeman, Z. Gecse, E. Gottschalk, L. Gray, D. Green, S. Grünendahl, O. Gutsche, J. Hanlon, R.M. Harris, S. Hasegawa, J. Hirschauer, Z. Hu, B. Jayatilaka, S. Jindariani, M. Johnson, U. Joshi, B. Klima, M.J. Kortelainen, B. Kreis, S. Lammel, D. Lincoln, R. Lipton, M. Liu, T. Liu, R. Lopes De Sá, J. Lykken, K. Maeshima, N. Magini, J.M. Marraffino, D. Mason, P. McBride, P. Merkel, S. Mrenna, S. Nahn, V. O'Dell, K. Pedro, O. Prokofyev, G. Rakness, L. Ristori, A. Savoy-Navarro[68], B. Schneider, E. Sexton-Kennedy, A. Soha, W.J. Spalding, L. Spiegel, S. Stoynev, J. Strait, N. Strobbe, L. Taylor, S. Tkaczyk, N.V. Tran, L. Uplegger, E.W. Vaandering, C. Vernieri, M. Verzocchi, R. Vidal, M. Wang, H.A. Weber, A. Whitbeck, W. Wu

University of Florida, Gainesville, USA
D. Acosta, P. Avery, P. Bortignon, D. Bourilkov, A. Brinkerhoff, A. Carnes, M. Carver, D. Curry, R.D. Field, I.K. Furic, S.V. Gleyzer, B.M. Joshi, J. Konigsberg, A. Korytov, K. Kotov, P. Ma, K. Matchev, H. Mei, G. Mitselmakher, K. Shi, D. Sperka, N. Terentyev, L. Thomas, J. Wang, S. Wang, J. Yelton

Florida International University, Miami, USA
Y.R. Joshi, S. Linn, P. Markowitz, J.L. Rodriguez

Florida State University, Tallahassee, USA
A. Ackert, T. Adams, A. Askew, S. Hagopian, V. Hagopian, K.F. Johnson, T. Kolberg, G. Martinez, T. Perry, H. Prosper, A. Saha, A. Santra, V. Sharma, R. Yohay

Florida Institute of Technology, Melbourne, USA
M.M. Baarmand, V. Bhopatkar, S. Colafranceschi, M. Hohlmann, D. Noonan, T. Roy, F. Yumiceva

University of Illinois at Chicago (UIC), Chicago, USA
M.R. Adams, L. Apanasevich, D. Berry, R.R. Betts, R. Cavanaugh, X. Chen, S. Dittmer,

O. Evdokimov, C.E. Gerber, D.A. Hangal, D.J. Hofman, K. Jung, J. Kamin, I.D. Sandoval Gonzalez, M.B. Tonjes, N. Varelas, H. Wang, Z. Wu, J. Zhang

The University of Iowa, Iowa City, USA
B. Bilki[69], W. Clarida, K. Dilsiz[70], S. Durgut, R.P. Gandrajula, M. Haytmyradov, V. Khristenko, J.-P. Merlo, H. Mermerkaya[71], A. Mestvirishvili, A. Moeller, J. Nachtman, H. Ogul[72], Y. Onel, F. Ozok[73], A. Penzo, C. Snyder, E. Tiras, J. Wetzel, K. Yi

Johns Hopkins University, Baltimore, USA
B. Blumenfeld, A. Cocoros, N. Eminizer, D. Fehling, L. Feng, A.V. Gritsan, W.T. Hung, P. Maksimovic, W. Qin, J. Roskes, U. Sarica, M. Swartz, M. Xiao, C. You

The University of Kansas, Lawrence, USA
A. Al-bataineh, P. Baringer, A. Bean, S. Boren, J. Bowen, J. Castle, S. Khalil, A. Kropivnitskaya, D. Majumder, W. Mcbrayer, M. Murray, C. Rogan, C. Royon, S. Sanders, E. Schmitz, J.D. Tapia Takaki, Q. Wang

Kansas State University, Manhattan, USA
A. Ivanov, K. Kaadze, Y. Maravin, A. Modak, A. Mohammadi, L.K. Saini, N. Skhirtladze

Lawrence Livermore National Laboratory, Livermore, USA
F. Rebassoo, D. Wright

University of Maryland, College Park, USA
A. Baden, O. Baron, A. Belloni, S.C. Eno, Y. Feng, C. Ferraioli, N.J. Hadley, S. Jabeen, G.Y. Jeng, R.G. Kellogg, J. Kunkle, A.C. Mignerey, F. Ricci-Tam, Y.H. Shin, A. Skuja, S.C. Tonwar

Massachusetts Institute of Technology, Cambridge, USA
D. Abercrombie, B. Allen, V. Azzolini, R. Barbieri, A. Baty, G. Bauer, R. Bi, S. Brandt, W. Busza, I.A. Cali, M. D'Alfonso, Z. Demiragli, G. Gomez Ceballos, M. Goncharov, P. Harris, D. Hsu, M. Hu, Y. Iiyama, G.M. Innocenti, M. Klute, D. Kovalskyi, Y.-J. Lee, A. Levin, P.D. Luckey, B. Maier, A.C. Marini, C. Mcginn, C. Mironov, S. Narayanan, X. Niu, C. Paus, C. Roland, G. Roland, G.S.F. Stephans, K. Sumorok, K. Tatar, D. Velicanu, J. Wang, T.W. Wang, B. Wyslouch, S. Zhaozhong

University of Minnesota, Minneapolis, USA
A.C. Benvenuti, R.M. Chatterjee, A. Evans, P. Hansen, S. Kalafut, Y. Kubota, Z. Lesko, J. Mans, S. Nourbakhsh, N. Ruckstuhl, R. Rusack, J. Turkewitz, M.A. Wadud

University of Mississippi, Oxford, USA
J.G. Acosta, S. Oliveros

University of Nebraska-Lincoln, Lincoln, USA
E. Avdeeva, K. Bloom, D.R. Claes, C. Fangmeier, F. Golf, R. Gonzalez Suarez, R. Kamalieddin, I. Kravchenko, J. Monroy, J.E. Siado, G.R. Snow, B. Stieger

State University of New York at Buffalo, Buffalo, USA
A. Godshalk, C. Harrington, I. Iashvili, D. Nguyen, A. Parker, S. Rappoccio, B. Roozbahani

Northeastern University, Boston, USA
G. Alverson, E. Barberis, C. Freer, A. Hortiangtham, A. Massironi, D.M. Morse, T. Orimoto, R. Teixeira De Lima, T. Wamorkar, B. Wang, A. Wisecarver, D. Wood

Northwestern University, Evanston, USA
S. Bhattacharya, O. Charaf, K.A. Hahn, N. Mucia, N. Odell, M.H. Schmitt, K. Sung, M. Trovato, M. Velasco

University of Notre Dame, Notre Dame, USA
R. Bucci, N. Dev, M. Hildreth, K. Hurtado Anampa, C. Jessop, D.J. Karmgard, N. Kellams, K. Lannon, W. Li, N. Loukas, N. Marinelli, F. Meng, C. Mueller, Y. Musienko[37], M. Planer, A. Reinsvold, R. Ruchti, P. Siddireddy, G. Smith, S. Taroni, M. Wayne, A. Wightman, M. Wolf, A. Woodard

The Ohio State University, Columbus, USA
J. Alimena, L. Antonelli, B. Bylsma, L.S. Durkin, S. Flowers, B. Francis, A. Hart, C. Hill, W. Ji, T.Y. Ling, W. Luo, B.L. Winer, H.W. Wulsin

Princeton University, Princeton, USA
S. Cooperstein, O. Driga, P. Elmer, J. Hardenbrook, P. Hebda, S. Higginbotham, A. Kalogeropoulos, D. Lange, J. Luo, D. Marlow, K. Mei, I. Ojalvo, J. Olsen, C. Palmer, P. Piroué, J. Salfeld-Nebgen, D. Stickland, C. Tully

University of Puerto Rico, Mayaguez, USA
S. Malik, S. Norberg

Purdue University, West Lafayette, USA
A. Barker, V.E. Barnes, S. Das, L. Gutay, M. Jones, A.W. Jung, A. Khatiwada, D.H. Miller, N. Neumeister, C.C. Peng, H. Qiu, J.F. Schulte, J. Sun, F. Wang, R. Xiao, W. Xie

Purdue University Northwest, Hammond, USA
T. Cheng, J. Dolen, N. Parashar

Rice University, Houston, USA
Z. Chen, K.M. Ecklund, S. Freed, F.J.M. Geurts, M. Guilbaud, M. Kilpatrick, W. Li, B. Michlin, B.P. Padley, J. Roberts, J. Rorie, W. Shi, Z. Tu, J. Zabel, A. Zhang

University of Rochester, Rochester, USA
A. Bodek, P. de Barbaro, R. Demina, Y.t. Duh, T. Ferbel, M. Galanti, A. Garcia-Bellido, J. Han, O. Hindrichs, A. Khukhunaishvili, K.H. Lo, P. Tan, M. Verzetti

The Rockefeller University, New York, USA
R. Ciesielski, K. Goulianos, C. Mesropian

Rutgers, The State University of New Jersey, Piscataway, USA
A. Agapitos, J.P. Chou, Y. Gershtein, T.A. Gómez Espinosa, E. Halkiadakis, M. Heindl, E. Hughes, S. Kaplan, R. Kunnawalkam Elayavalli, S. Kyriacou, A. Lath, R. Montalvo, K. Nash, M. Osherson, H. Saka, S. Salur, S. Schnetzer, D. Sheffield, S. Somalwar, R. Stone, S. Thomas, P. Thomassen, M. Walker

University of Tennessee, Knoxville, USA
A.G. Delannoy, J. Heideman, G. Riley, K. Rose, S. Spanier, K. Thapa

Texas A&M University, College Station, USA
O. Bouhali[74], A. Castaneda Hernandez[74], A. Celik, M. Dalchenko, M. De Mattia, A. Delgado, S. Dildick, R. Eusebi, J. Gilmore, T. Huang, T. Kamon[75], R. Mueller, Y. Pakhotin, R. Patel, A. Perloff, L. Perniè, D. Rathjens, A. Safonov, A. Tatarinov

Texas Tech University, Lubbock, USA
N. Akchurin, J. Damgov, F. De Guio, P.R. Dudero, J. Faulkner, E. Gurpinar, S. Kunori, K. Lamichhane, S.W. Lee, T. Mengke, S. Muthumuni, T. Peltola, S. Undleeb, I. Volobouev, Z. Wang

Vanderbilt University, Nashville, USA
S. Greene, A. Gurrola, R. Janjam, W. Johns, C. Maguire, A. Melo, H. Ni, K. Padeken, J.D. Ruiz Alvarez, P. Sheldon, S. Tuo, J. Velkovska, Q. Xu

University of Virginia, Charlottesville, USA
M.W. Arenton, P. Barria, B. Cox, R. Hirosky, M. Joyce, A. Ledovskoy, H. Li, C. Neu, T. Sinthuprasith, Y. Wang, E. Wolfe, F. Xia

Wayne State University, Detroit, USA
R. Harr, P.E. Karchin, N. Poudyal, J. Sturdy, P. Thapa, S. Zaleski

University of Wisconsin - Madison, Madison, WI, USA
M. Brodski, J. Buchanan, C. Caillol, D. Carlsmith, S. Dasu, L. Dodd, S. Duric, B. Gomber, M. Grothe, M. Herndon, A. Hervé, U. Hussain, P. Klabbers, A. Lanaro, A. Levine, K. Long, R. Loveless, V. Rekovic, T. Ruggles, A. Savin, N. Smith, W.H. Smith, N. Woods

†: Deceased
1: Also at Vienna University of Technology, Vienna, Austria
2: Also at IRFU; CEA; Université Paris-Saclay, Gif-sur-Yvette, France
3: Also at Universidade Estadual de Campinas, Campinas, Brazil
4: Also at Federal University of Rio Grande do Sul, Porto Alegre, Brazil
5: Also at Universidade Federal de Pelotas, Pelotas, Brazil
6: Also at Université Libre de Bruxelles, Bruxelles, Belgium
7: Also at Institute for Theoretical and Experimental Physics, Moscow, Russia
8: Also at Joint Institute for Nuclear Research, Dubna, Russia
9: Also at Cairo University, Cairo, Egypt
10: Now at Ain Shams University, Cairo, Egypt
11: Also at Fayoum University, El-Fayoum, Egypt
12: Now at British University in Egypt, Cairo, Egypt
13: Also at Department of Physics; King Abdulaziz University, Jeddah, Saudi Arabia
14: Also at Université de Haute Alsace, Mulhouse, France
15: Also at Skobeltsyn Institute of Nuclear Physics; Lomonosov Moscow State University, Moscow, Russia
16: Also at CERN; European Organization for Nuclear Research, Geneva, Switzerland
17: Also at RWTH Aachen University; III. Physikalisches Institut A, Aachen, Germany
18: Also at University of Hamburg, Hamburg, Germany
19: Also at Brandenburg University of Technology, Cottbus, Germany
20: Also at MTA-ELTE Lendület CMS Particle and Nuclear Physics Group; Eötvös Loránd University, Budapest, Hungary
21: Also at Institute of Nuclear Research ATOMKI, Debrecen, Hungary
22: Also at Institute of Physics; University of Debrecen, Debrecen, Hungary
23: Also at Indian Institute of Technology Bhubaneswar, Bhubaneswar, India
24: Also at Institute of Physics, Bhubaneswar, India
25: Also at Shoolini University, Solan, India
26: Also at University of Visva-Bharati, Santiniketan, India
27: Also at University of Ruhuna, Matara, Sri Lanka
28: Also at Isfahan University of Technology, Isfahan, Iran
29: Also at Yazd University, Yazd, Iran
30: Also at Plasma Physics Research Center; Science and Research Branch; Islamic Azad University, Tehran, Iran
31: Also at Università degli Studi di Siena, Siena, Italy

32: Also at INFN Sezione di Milano-Bicocca; Università di Milano-Bicocca, Milano, Italy

33: Also at International Islamic University of Malaysia, Kuala Lumpur, Malaysia

34: Also at Malaysian Nuclear Agency; MOSTI, Kajang, Malaysia

35: Also at Consejo Nacional de Ciencia y Tecnología, Mexico city, Mexico

36: Also at Warsaw University of Technology; Institute of Electronic Systems, Warsaw, Poland

37: Also at Institute for Nuclear Research, Moscow, Russia

38: Now at National Research Nuclear University 'Moscow Engineering Physics Institute' (MEPhI), Moscow, Russia

39: Also at St. Petersburg State Polytechnical University, St. Petersburg, Russia

40: Also at University of Florida, Gainesville, USA

41: Also at P.N. Lebedev Physical Institute, Moscow, Russia

42: Also at California Institute of Technology, Pasadena, USA

43: Also at Budker Institute of Nuclear Physics, Novosibirsk, Russia

44: Also at Faculty of Physics; University of Belgrade, Belgrade, Serbia

45: Also at INFN Sezione di Pavia; Università di Pavia, Pavia, Italy

46: Also at University of Belgrade; Faculty of Physics and Vinca Institute of Nuclear Sciences, Belgrade, Serbia

47: Also at Scuola Normale e Sezione dell'INFN, Pisa, Italy

48: Also at National and Kapodistrian University of Athens, Athens, Greece

49: Also at Riga Technical University, Riga, Latvia

50: Also at Universität Zürich, Zurich, Switzerland

51: Also at Stefan Meyer Institute for Subatomic Physics (SMI), Vienna, Austria

52: Also at Adiyaman University, Adiyaman, Turkey

53: Also at Istanbul Aydin University, Istanbul, Turkey

54: Also at Mersin University, Mersin, Turkey

55: Also at Piri Reis University, Istanbul, Turkey

56: Also at Gaziosmanpasa University, Tokat, Turkey

57: Also at Izmir Institute of Technology, Izmir, Turkey

58: Also at Necmettin Erbakan University, Konya, Turkey

59: Also at Marmara University, Istanbul, Turkey

60: Also at Kafkas University, Kars, Turkey

61: Also at Istanbul Bilgi University, Istanbul, Turkey

62: Also at Rutherford Appleton Laboratory, Didcot, United Kingdom

63: Also at School of Physics and Astronomy; University of Southampton, Southampton, United Kingdom

64: Also at Monash University; Faculty of Science, Clayton, Australia

65: Also at Instituto de Astrofísica de Canarias, La Laguna, Spain

66: Also at Bethel University, ST. PAUL, USA

67: Also at Utah Valley University, Orem, USA

68: Also at Purdue University, West Lafayette, USA

69: Also at Beykent University, Istanbul, Turkey

70: Also at Bingol University, Bingol, Turkey

71: Also at Erzincan University, Erzincan, Turkey

72: Also at Sinop University, Sinop, Turkey

73: Also at Mimar Sinan University; Istanbul, Istanbul, Turkey

74: Also at Texas A&M University at Qatar, Doha, Qatar

75: Also at Kyungpook National University, Daegu, Korea